A steadily flowing glacier and no detectable precursor before the 11 October 2026 Budhi Gandaki rock–ice avalanche and flood, Nepal

Ajay Kumar Sah

Purbanchal University School of Engineering, Biratnagar, Nepal

Correspondence: Ajay Kumar Sah (ajayshah2005@gmail.com)
ORCID: https://orcid.org/0009-0004-8543-4306

This is a non-peer-reviewed preprint submitted to EarthArXiv.
It has not been submitted to a peer-reviewed journal.

Version 2, 30 October 2026 (version 1: 15 October 2026)

A steadily flowing glacier and no detectable precursor before the 11 October 2026 Budhi Gandaki rock–ice avalanche and flood, Nepal

Ajay Kumar Sah
Purbanchal University School of Engineering, Biratnagar, Nepal; ajayshah2005@gmail.com

Abstract

On 11 October 2026 at about 04:20 local time, a rock–ice avalanche at the head of the Ungilung Khola, on the southern slopes of Chamar (7,165 m) in Gorkha District, Nepal, became a debris flow and flood that travelled down the Syar Khola and the Budhi Gandaki. I reconstruct the event from free satellite data (Sentinel-1, Sentinel-2, Landsat 8/9, ITS_LIVE and NISAR), official records and my own reading of historical Google Earth imagery. Version 1 covered the first four days; this version adds the first clear Sentinel-2 images (21–26 October) and post-event radar. Each change test is compared with a control, where possible a fake event made from images taken before the event. The change mapped at the source on 11 October happened between 6 October 10:41 and 11 October 10:42 local time. A river gauge 23 km downstream recorded no flood pulse between 5 and 11 October. On 13 October, Landsat 9 shows a 0.31 km² block of snow loss at 5,020–5,470 m on an unnamed valley glacier, absent in the fake test, and a candidate avalanche track at 6,350–6,600 m above face B; face A is unchanged. The glacier had flowed at about 60–130 m yr^{-1} for a decade, and no speed-up or other precursor was detected. Newly public L-band interferograms from NISAR kept face B within about ±2 cm along the line of sight in every pair from May to 7 October, and showed nothing unusual on the hanging glacier above it in the pair that ended 9.5 hours before the collapse. Against 1 October, the clear images show a 0.85–1.03 km² dark area at the head, centred on the 0.21 km² snow → grey patch of version 1, where bright snow had turned to a dark surface, most likely debris or dust (0.55 km² against the same day in 2025); face A was as in October 2025. About 20 km² of ground changed from the head to the Syar confluence, against 8.4 km² in the same weeks of 2025. Across the event, NISAR coherence fell on 13–18 % of the path below 4,000 m on all three tracks, against at most 6–10 % in earlier pairs, but it did not outline the source. Radar at 06:03 recorded a fresh rough surface, most likely deposit or debris-laden water, 0.5–1.5 km up the Syar Khola from its confluence with the Ungilung, where the blockage and a 1.5 km backwater were reported. The flood reached Arughat, 63 river km downstream, in at least three rises, the largest last. The release scar, its volume and any chain of small lakes remain unmeasured without high-resolution imagery or a post-event elevation model.

Keywords: Budhi Gandaki; Ungilung; Gorkha; Nepal; rock–ice avalanche; debris flow; landslide dam; glacier velocity; ITS_LIVE; Sentinel-1; Sentinel-2; Landsat 9; NISAR; L-band InSAR; precursor

Version 2 (30 October 2026). Changes from version 1 (15 October 2026): (1) new Sect. 3.8 with the first clear Sentinel-2 images after the event (21, 23 and 26 October), a 2025 same-season control, and the Budhi Gandaki valley floor at the Yaru Khola mouth; (2) new Sect. 3.9 with NISAR coherence across the event on three tracks; (3) the Sentinel-1 ascending pair 3 → 15 October, which does not repeat the descending coherence loss on face B, so the face B coherence result is softened (Sect. 3.2, Table 1); (4) ERA5 for 10–12 October (Sect. 4.1); the ERA5 total for 1–9 October now reads 21.0 mm instead of 21.5 mm; (5) updated Sects. 4.3, 4.4 and 5. All version 1 results are otherwise unchanged.

1 Introduction

Rock and ice avalanches in high mountains can turn into debris flows that travel tens of kilometres and cause damage far from their source. The 7 February 2021 Chamoli disaster in the Indian Himalaya is the best documented recent case: about 27×10^6 m³ of rock and glacier ice fell from Ronti Peak and became a highly mobile debris flow (Shugar et al., 2021). In the Budhi Gandaki basin of central Nepal, an ice avalanche from the Manaslu Glacier into Birendra Tal caused a displacement-wave flood on 21 April 2024 (Maharjan et al., 2024). On 26 August 2026, a rock–ice avalanche at Langtang Lirung, about 65 km to the south-east, caused the Gyirong–Rasuwa disaster (ICIMOD, 2026). It was the subject of my earlier studies on what routine satellite products can detect before such failures (Sah, 2026a, b, c, d).

On 11 October 2026, a second large event in this region began at the head of the Ungilung Khola, a north-side tributary of the Syar Khola in Chumnubri Rural Municipality, Gorkha District. The resulting flood swept away a hydropower camp at Salleri, damaged four hydropower projects under construction and destroyed the river gauge at Arughat (NDRRMA, 2026a; HWRRC, 2026; SANDRP, 2026). Five people staying in a shed on the banks of the Ungilung were reported missing (Uprety et al., 2026). The National Disaster Risk Reduction and Management Authority (NDRRMA) released a technical report on 12–13 October, describing a snow avalanche at about 6,000 m and a landslide that included glacier ice at about 5,500 m (NDRRMA, 2026b; Onlinekhabar, 2026). ICIMOD stated that satellite imagery had confirmed an ice–rock avalanche and glacier collapse in the basin (ICIMOD, 2026).

The source area was under cloud on the morning of the event, and no clear 10 m optical image had been acquired

four days later. This is a common situation after Himalayan disasters in the post-monsoon season. It raises a practical question: what can free satellite data, official records and careful image reading establish before a clear image arrives, and with what confidence?

In this preprint I answer that question for the Ungilung event. I combine free satellite data, the official gauge and situation reports, and my own reading of historical Google Earth imagery of the source glacier. I treat each satellite result as a test with a control. Where possible, a change map is compared with the same map made from a pair of images taken before the event (a "fake event"). The aims are to establish (1) the timing of the collapse, (2) where the source was, (3) the state of the glacier before the event and whether any precursor was visible, (4) how far up the valley walls the flow reached, (5) where and when the river was blocked, and (6) how the flood travelled downstream. I also record which tests failed or gave misleading results, because these are lessons for the next rapid assessment.

2 Study area, data and methods

2.1 Setting

The Ungilung Khola drains south from the ridge below Chamar (7,165 m; 28.5553° N, 84.9453° E), which is usually given as the highest peak of the Sringi (Serang) Himal. The NDRRMA report places the source between Chamar Himal and Syerangi Himal (NDRRMA, 2026b; Fig. 1). Its head holds an unnamed valley glacier, mapped in the Randolph Glacier Inventory as RGI60-15.04014 and RGI2000-v7.0-G-15-05404 (RGI Consortium, 2017; RGI 7.0 Consortium, 2023). In those outlines (source images 1998–2002) the glacier covers 1.5 km² between 4,380 and 5,910 m, faces south-west (217–221°) and is 2.3–2.7 km long, with a mean slope of 31–33°. A small, steep hanging glacier (RGI 7 G-15-05405; 0.74 km², 5,510–6,620 m, slope 43°) lies above it to the north-west.

I use two names for the steep walls above the glacier. **Face A** is a broad south-facing wall at 5,860–6,370 m (0.58 km², centre 28.5380° N, 84.9445° E), directly above the upper glacier. **Face B** is a smaller and steeper rock wall at 5,920–6,410 m (0.07 km², slope about 59°, centre 28.5348° N, 84.9314° E), about 1.2 km to the west-south-west, below the hanging glacier. Both faces were defined on 13 October from the first change maps, before most of the tests reported here.

The downhill routes from faces A and B meet at about 4,800 m (28.5243° N, 84.9326° E), at the western margin of the glacier. The glacier tongue continues to about 4,380 m in the RGI outline. Below it the valley narrows to a gorge at about 4,100 m (28.5156° N, 84.9289° E), where the valley is 130 m wide at 30 m above the stream. From the 4,800 m meeting point, the Ungilung falls about 2,810 m over 8.1 km (mean gradient 35 %) to its confluence with the south-west-flowing Syar Khola at about 1,990 m (28.4637° N, 84.9429° E). The Syar joins the Budhi Gandaki about 7 km further downstream. The Ungilung catchment above the confluence covers about 25 km². About 10 % of it is glacier in the RGI 7 outlines (2.4 km²), and the valley glacier is the largest of these (1.5 km²). Besides the glacier stream, at least six side streams, each draining 1–4.5 km², join the Ungilung below the glacier. The Budhi Gandaki then flows south past Salleri, Jagat and Machha Khola to Arughat. I measure distances along this route as river kilometres from the 4,800 m meeting point (km 0). The source faces lie about 1.5–2 km upslope of km 0. The Ungilung–Syar confluence is at km 8.1, the Syar–Budhi Gandaki confluence at km 14.9, Salleri at km 22.6 and Arughat at km 63.

2.2 Data

- **Sentinel-2** Level-2A surface reflectance (10–20 m) for 2023–2026, including 1, 3, 6 and 11 October 2026 (the 11 October scene was acquired at 10:42 NPT, about 6 h after the event), and 6, 11 and 21 October 2025 for fake-event tests, accessed through the Microsoft Planetary Computer (Microsoft Open Source et al., 2022). For version 2 I add the first clear scenes after the event (21 October 2026, Sentinel-2C; 23 October, Sentinel-2A; 26 October, Sentinel-2B; tile 45RTM) and 6, 21 and 26 October 2025 for the same-season control. All scenes of Sect. 3.8, including 1 October 2026, were read from the Earth Search catalogue (Element 84, 2023).
- **Landsat 8 and 9.** Collection 2 Level-2 scenes of 4 and 5 October 2026 (Planetary Computer). Landsat 9 Collection 2 Level-1 scene LC09_L1TP_141040_20261013_20261013_02_T1 (13 October 2026, 10:33 NPT, scene cloud 10.3 %), which I downloaded from USGS EarthExplorer and converted to top-of-atmosphere reflectance using its metadata file.
- **Sentinel-1** radiometrically terrain-corrected backscatter (descending track 19; nine passes from 7 July to 11 October 2026; the last at 06:03 NPT on 11 October), from the Planetary Computer.
- **Sentinel-1 interferometric products** (12-day pairs, descending track 19 and ascending track 85, June to 15 October 2026, including the ascending event pair 3 → 15 October) processed on demand with ASF HyP3 (Hogenson et al., 2020).
- **NISAR** L-band (24 cm wavelength) provisional geocoded interferograms (GUNW; 12-day pairs, three of them 24-day; HH polarisation; wrapped phase and coherence at 20 m) from May to 10 October 2026: ascending track 98 (about 05:24 NPT), descending tracks 149 and 48 (18:51 and 18:43 NPT). The last pre-event pairs end on 3

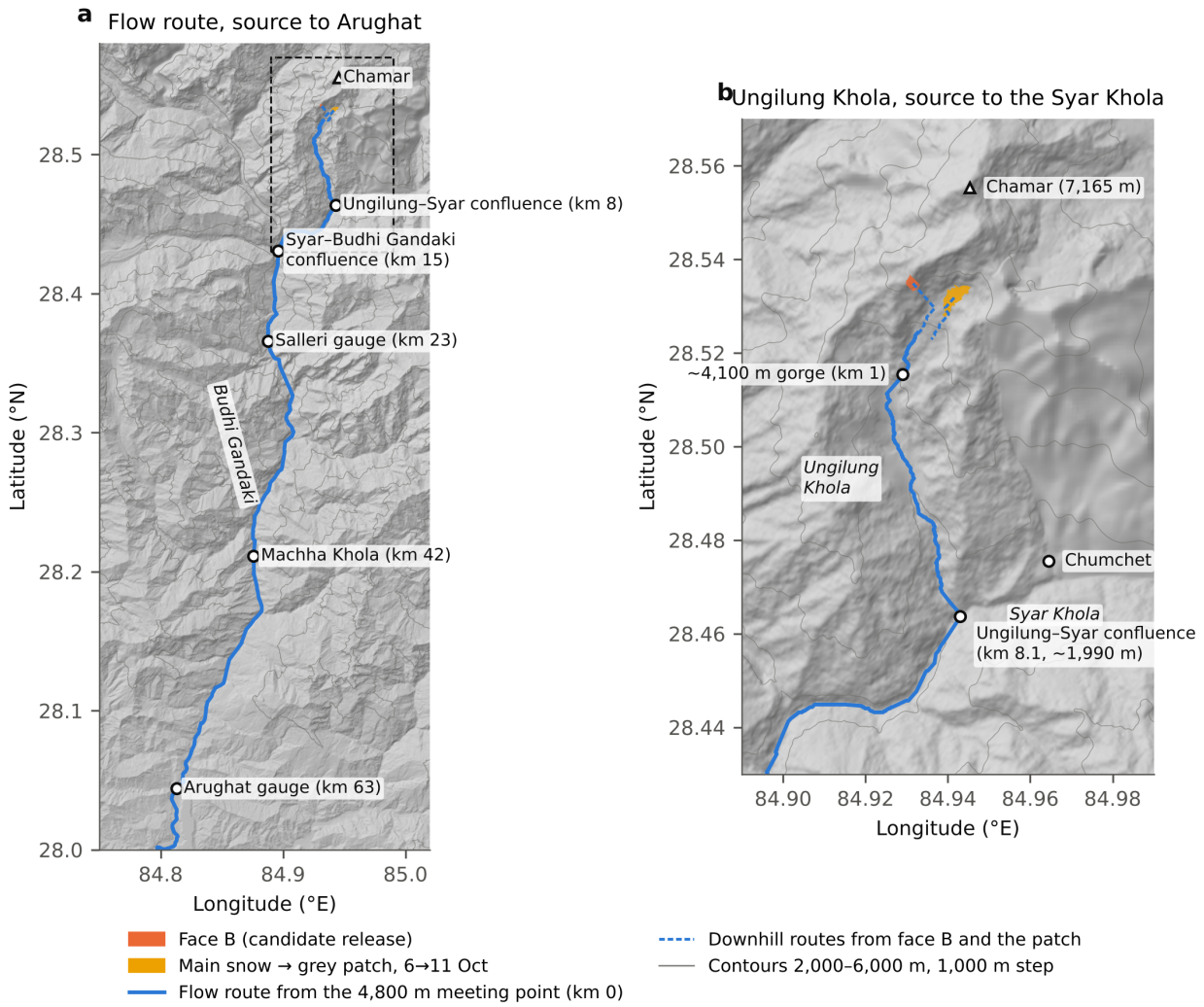


Figure 1. Location. (a) Flow route from the 4,800 m meeting point of the routes from faces A and B (km 0) to Arughat (km 63) on a GLO-30 hillshade, with river kilometres of the confluences and gauges. (b) The Ungilung Khola from the source to the Syar Khola. Orange: face B; yellow: the main snow → grey patch of 6 → 11 October (Sentinel-2); dashed blue: downhill routes from face B and from the patch. Contours every 1,000 m.

October (track 48), 7 October 05:24 (track 98) and 10 October 18:51 (track 149), 9.5 h before the collapse. For version 2, the first pair across the event on each track: 3 → 15 October (track 48), 7 → 19 October NPT (track 98; 6 → 18 October UTC) and 10 → 22 October (track 149). Products are from the Alaska Satellite Facility (NASA/JPL NISAR Project, 2026); I read only a small area around the source from each file.

- **ERA5** daily temperature, precipitation and snowfall for 2014 to 12 October 2026 at the grid point nearest the source (Hersbach et al., 2020), through the Open-Meteo archive (Zippenfenig, 2024).
- **ITS_LIVE** glacier velocities from individual image pairs (84,550 pairs from Landsat 4–9, Sentinel-1 and Sentinel-2) read from the ITS_LIVE version 2 data cube (Gardner et al., 2018; ITS_LIVE, 2026).
- **Copernicus GLO-30 DEM** (ESA, 2022) for elevation, slope and flow routing.
- **Google Earth historical imagery** of the source glacier (2006, 2008, 2012, 2016 and January 2026), which I inspected by eye (Sect. 2.3.4), and the true-colour view of the Sentinel-2 images of 12 August, 6, 11 and 21 October 2026 in the Copernicus Browser (Copernicus Data Space Ecosystem, 2026), which I also inspected by eye (Sect. 3.8).
- **Official records:** NDRRMA Situation Report 1 (NDRRMA, 2026a); the NDRRMA technical report on the flood, published on the Authority's Facebook page with figures of the Salleri river gauge, a location map and a drone mosaic of the Ungilung–Syar confluence (NDRRMA, 2026b); and Situation Report 1 of the Flood Forecasting Division of the Hydrology and Water Resources Research Centre, with the Arughat gauge record and flood volumes (HWRRC, 2026).
- **News and eyewitness reports**, used only for times and places that I could check against a second source (Sect. 3.1).

All times are Nepal Standard Time (NPT, UTC + 5:45).

2.3 Methods

2.3.1 Change tests with fake-event controls

I map snow with the normalised difference snow index (NDSI) from the green and shortwave-infrared (SWIR1) bands: a pixel is snow if NDSI > 0.4 and green reflectance > 0.15 (> 0.2 in the pixel tests of Sentinel-2). For Sentinel-2 I exclude cloud and cloud shadow with the scene classification layer. For a stricter "snow → rock" test I require the snow index to fall below 0.2 and SWIR1 reflectance to at least double. For the deposit in the valley I use a "deposit-type" test: NDVI above 0.4 before and below 0.25 after, with NIR and SWIR1 both falling to 0.6 times their earlier value or less. For the run-up band (Sect. 3.5) I use a looser vegetation-loss test: a drop in the normalised difference vegetation index (NDVI) of more than 0.15 on pixels that had NDVI > 0.3 before the event.

For the source area I use an 80 m grid. In each cell I compute the fraction of clear pixels that changed from snow to not snow. A cell is flagged when this fraction is above the 97.5th percentile of control cells. Control cells lie above 5,000 m and outside faces A and B and the mapped change patches. Clusters of flagged cells are then compared with the same grid computed from a pair of images taken before the event. A cluster that appears in the event pair but not in the fake pair is treated as event-related.

For Landsat 9 on 13 October I use the same band pair as Landsat 8 (green and SWIR1, bands 3 and 6). The event pair is Landsat 8 on 5 October → Landsat 9 on 13 October; the fake pair is Landsat 9 on 4 October → Landsat 8 on 5 October. The two pairs are not identical in three ways. The 13 October scene is top-of-atmosphere reflectance (Level-1), while the others are surface reflectance (Level-2). For 13 October I mask only the high-confidence cloud bit of the quality band (Sect. 4.3), while for 4 and 5 October the cloud, cloud-shadow and dilated-cloud bits are masked. The fake pair spans one day and the event pair eight days. The thresholds are set separately in each pair from its own control cells, which absorbs part of these differences.

For version 2 I use two further rules on Sentinel-2 surface reflectance (10 m). The **dark-area rule**, applied only to images clear over the head, marks pixels that were bright before (red reflectance > 0.30) and dark after (red < 0.12), with blue/red < 0.95 after, so that shadowed snow, which is bluish, is not counted. I remove single-pixel specks with a morphological opening, keep the connected patches that touch a 600 m circle around the centre of the 0.21 km² snow → grey patch of Sect. 3.2 (the main block), and fill holes. The **path-change rule** excludes cloud, cloud shadow and no-data on both dates with the scene classification layer. It marks a pixel as changed if bright snow or ice turned dark (the same red thresholds), if vegetation was lost (NDVI > 0.30 before and a drop of more than 0.20), or if bare ground changed strongly (red change > 0.08 with NDVI change < 0.1, outside snow), and keeps patches of at least 2 ha. I compare 1 → 21 October 2026 with the same weeks of 2025 (6 → 26 October 2025) as a same-season control.

2.3.2 Radar backscatter, coherence and L-band interferometry

For backscatter I average VV and VH in decibels over each target area and compare each pass with the same area's earlier passes and with control areas. For coherence I use the median coherence and the fraction of pixels below 0.15 in each target area (the method of Sah, 2026b). I compare the event pair (29 September → 11 October) with the two earlier pairs and with 593 steep control windows at the same height.

For NISAR I use the wrapped interferogram at 20 m. I keep pixels with coherence above 0.3 that are not in radar layover or shadow, which I compute from the GLO-30 slope and aspect with an estimated look geometry for each track (heading and incidence angle from the frame position). Face B faces south-south-east (about 151°). The descending tracks, which look east, see it at a grazing angle (61 % shadow on track 149), while ascending track 98 sees it at a local incidence of about 57°. The hanging glacier faces west-south-west (about 253°) and is seen best by descending track 149. I remove the part of the phase that follows elevation, mostly water vapour in the lower atmosphere, by referencing each 100 m elevation band to control pixels at the same height that lie more than 300 m from the source. I then average the residual phase over fixed outlines (face A, face B, the main block and the hanging glacier) and convert it to line-of-sight (LOS) displacement; one cycle of phase is 12 cm. Each value is compared with 300 random patches of similar size on steep ground above 5,300 m in the same pair, and each target's last pre-event pair is compared with its own earlier pairs.

NISAR coherence across the event. For each track I compare the coherence of the first pair across the event with all pairs of the same track from 1 June 2026 to the event (7, 9 and 7 pairs on tracks 48, 98 and 149; all 12-day except one 24-day pair per track), on the native 20 m grid. For each pixel I compute a robust score, the event coherence minus the pre-event median, divided by 1.4826 times the median absolute deviation (at least 0.03). A pixel counts as a loss if the score is −3 or lower and the coherence fell by at least 0.2, and only where the pre-event median is at least 0.3. I report the share of loss pixels in the Sentinel-2 path-change zone (its outline, with holes filled, 21.0 km²), in the dark area of Sect. 3.8 and in a control zone more than 1.5 km from both (overall and below 4,000 m), and I run the same test on

each pre-event pair, leaving it out of the reference, to find the share expected by chance.

2.3.3 Glacier velocity

From the ITS_LIVE data cube I extracted every image pair at two points in the fast-flowing part of the glacier (84.9380° E, 28.5290° N and 84.9395° E, 28.5300° N) and at a stable rock point (84.9270° E, 28.5280° N). For each set of pairs I take the median of the east and north velocity components separately and combine them (a vector median). This reduces the effect of individual mismatches. I group pairs by length, by year and by sensor.

As an independent check, I tracked features in Sentinel-2 red and near-infrared bands with phase correlation (Guizar-Sicairos et al., 2008; van der Walt et al., 2014), using 320 m windows on the glacier. I removed any image-wide shift using stable rock. I tested significance against the 95th percentile of offsets measured on windows of stable rock of the same size. For face B, which is small, I used 48-pixel patches and compared them with 87 steep control patches.

2.3.4 Google Earth inspection

I placed pins on recognisable surface features of the glacier (pits, cracks and a rock block) in the November 2016 image, and on the features I judged to be the same in the January 2026 image. The ITS_LIVE annual composites had already been extracted at that time. I placed the pins with the ITS_LIVE layer hidden and matched features by their shape. I also pinned a rock spur on the glacier margin (84.9418° E, 28.5288° N) on four dates as a control for image misregistration. I marked the upper edge of the zone where the glacier surface breaks up on the 2006, 2008, 2016 and 2026 images. These pins are by eye, and their precision is about 5–10 m on a rock knob and 10–25 m on a diffuse edge.

2.3.5 Routing, run-up and flood timing

I traced flow routes downhill on the GLO-30 DEM with a priority-flood search and measured river kilometres along them. For pixels that lost vegetation on 11 October, I computed the height above the nearest channel cell. I combined gauge times, report times and route distances into average travel speeds. These are averages over long reaches, limited by the timing precision of each source.

2.3.6 Use of AI-assisted technology

The analysis code used to produce the results and figures reported here, and the initial drafting of this manuscript, were produced with assistance from Claude (Anthropic), a large language model, in interactive sessions during October 2026. The model was used to write the processing and statistical code, to generate the figures, to search for and translate news reports and official documents, to check the cited sources, and to draft text. The study design, the Google Earth and Copernicus Browser observations, the hypotheses and the interpretation of results are the author's. The author has verified the reported values by running the accompanying scripts, archived with the derived data on Zenodo (Sah, 2026e), and accepts full responsibility for the content.

3 Results

3.1 Timing

The collapse happened at about 04:20 on 11 October (Fig. 2a). The NDRRMA technical report gives about 04:20 (NDRRMA, 2026b; Onlinekhabar, 2026), and a seismic signal was recorded at 04:22 (K. Cook, reported by Petley, 2026). A local call at 04:45 from Ghattekhola, above Sirdibas, reported that a landslide had blocked the river, and a flood warning was posted on Facebook at 04:59 (Kathmandu Post, 2026). NDRRMA Situation Report 1 gives "around 5:30 am" (NDRRMA, 2026a). Given the seismic record and the local warnings, I read this as the time the event was reported, not the time it began. The NDRRMA technical report also states that several smaller landslides occurred before and after the main one (NDRRMA, 2026b). The satellite data cannot date these.

The satellite data bracket the change at the source independently:

- **Before 6 October, nothing changed.** In the source area, the strict snow → rock test finds 0.000 km² between 3 and 6 October and 0.007 km² between 1 and 6 October, on about 2.5 km² of pixels that were clear on both dates. The main change patch (Sect. 3.2) was 100 % snow on Landsat 8 at 10:32 on 5 October and 99 % snow on Sentinel-2 at 10:41 on 6 October. Down the valley, the deposit-type change (vegetation to flat grey) covered 0.001–0.002 km² between 1, 3 and 6 October.
- **By 10:42 on 11 October, the change had happened.** Between 6 and 11 October, 0.26 km² of snow turned to a rock-like surface at the head (20 % of the clear area), and 1.18 km² of vegetation turned grey down the valley (16 % of the clear area).

- **Radar agrees.** On the ascending pair 21 September → 3 October, face B kept a coherence of 0.59, against 0.30 for steep control slopes, so face B had not changed by 3 October.

The Salleri gauge of the Budhi Gandaki hydropower project, at river km 22.6, recorded a smooth recession from 5 to 11 October, with only a small rise of about 0.09 m on the evening of 9 October. There is no rise or fall before the record ends at about 04:30–04:40 on 11 October, when the gauge was damaged by the flood (NDRRMA, 2026b). So no earlier flood pulse passed Salleri in the six days before the event.

An analyst at ICIMOD first proposed that a rock avalanche had occurred “most likely on Oct. 5” (Bikas, 2026; as reported by SANDRP, 2026). My tests find no change on 5 or 6 October on the glacier, in the valley or in the river. The Sentinel-2 change at the head and down the valley, the seismic signal and the first local reports all fall between 6 October 10:41 and the early morning of 11 October. The Landsat 9 results (Sect. 3.2) are bracketed only to 5–13 October. A small fall from face B before 6 October cannot be fully excluded, because face B itself was under cloud on 6 October (Sect. 3.2). However, it did not leave debris on the snow below.

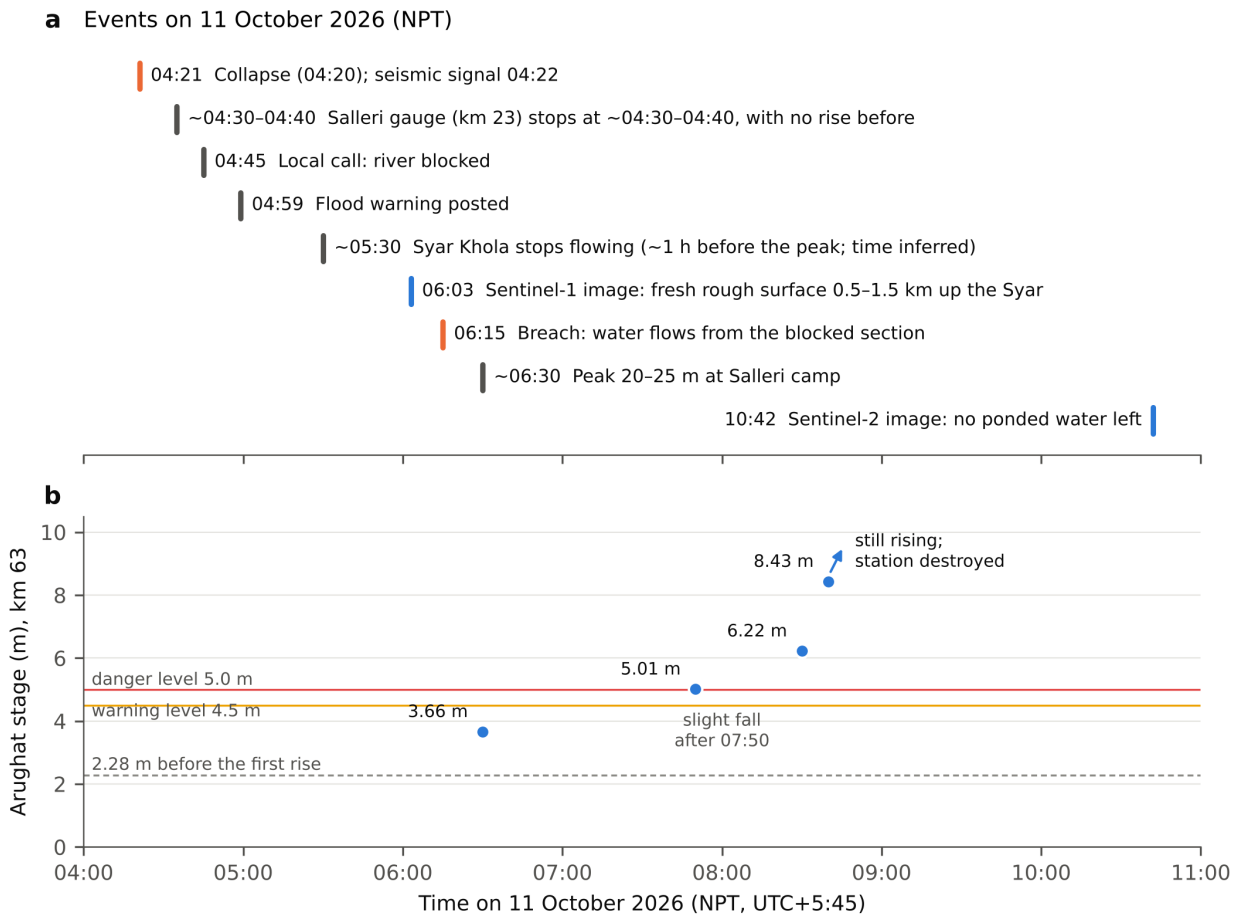


Figure 2. (a) Events on 11 October 2026, from the seismic record (Petley, 2026), NDRRMA (2026a, b), the Kathmandu Post (2026) and this study (blue). The end of the Salleri record is given as about 04:30–04:40. The time the Syar stopped flowing is inferred from “about one hour before the largest level”. (b) Arughat gauge readings (HWRRC, 2026). The report states that the level fell slightly after 06:30 and after 07:50; these falls were not given as values and are not plotted.

3.2 Source area

Several lines of evidence, from three sensors and from independent analyses, place the release on the face B side of the headwall and show that face A did not fail (Table 1, Figs. 3 and 4).

Sentinel-2, 1 and 6 → 11 October. The largest change between 6 and 11 October is a 0.21 km² patch at 5,160–5,550 m on the upper valley glacier (centre 28.5319° N, 84.9415° E), where snow turned to a flat grey, rock-like surface. Face B was mostly cloudy on 6 October, so for it I use 1 October as the earlier date. Between 1 and 11 October a smaller patch (0.05 km², about 5,500–5,950 m) appeared directly below face B, and 19 % of clear pixels on face B itself passed the strict snow → rock test, against 0.0 % of 18,403 pixels on other steep faces at the same height. Face A showed no snow loss. Across the region, 2 km cells at 5,000–6,000 m lost 0–6 % of their snow, and a few cells lost up to 17 %. The three cells at the head lost 96 %, 63 % and 42 %.

Height of the highest change. Snow loss on the face B column begins at 6,200–6,300 m (16 % of snow pixels), rises to 57 % at 6,100–6,200 m and 97 % at 6,000–6,100 m. On the face A column, loss is at most 6 % above 6,000 m and begins only at the foot of the wall (30 % at 5,900–6,000 m). Control areas at the same heights lost at most 5 % above 5,300 m. The highest change is therefore on the face B side, about 6,100–6,300 m.

Radar coherence. Face B is the only target with a clear drop in coherence on the event pair (descending, 29 September → 11 October): from a pre-event mean of 0.21 to 0.10. This is the lowest value in its nine-pair record, whose earlier minimum was 0.18. Of 593 steep control windows at 5,800–6,400 m, 1.9 % dropped as much and 0.2 % ended as low. One pair earlier, with no event, face B changed by +0.04. Face A rose from 0.22 to 0.26. The test rests on only 43 pixels, and the rest of the head is at the coherence noise floor (about 0.2) before and after (Sect. 4.3). In an 80 m grid test the face B cells were not flagged. The ascending event pair (3 → 15 October), which became available after version 1, does not repeat the loss: face B fell from 0.36 (mean of the two previous pairs) to 0.20, but its ascending record ranges from 0.15 to 0.81, its difference from steep control slopes in the event pair (−0.03) was lower than in only 3 of 7 earlier pairs, and 10.8 % of 74 steep windows dropped as much. So the descending result is consistent with face B but is not confirmed by the second geometry, and it should not be given weight on its own. On the same ascending pair, the lower Ungilung route and the confluence were lower against their valley control than in any of eight pairs, but only slightly, and a map of strong losses covered less area (3.1 km²) than in two pairs without an event (5.7 and 13.3 km²); C-band ascending coherence shows neither the source nor the deposit.

Landsat 9, 5 → 13 October (grid test). With matched bands, the largest cluster of flagged cells covers 49 cells (0.31 km²) at 5,020–5,470 m (centre 28.5292° N, 84.9398° E; Fig. 4a). It covers the Sentinel-2 grey patch and the fast-flowing glacier below it, down to the break in slope at about 5,000 m (Sect. 3.3). Its median snow loss is 1.00 in the event pair and 0.00 in the fake pair, where none of its 46 valid cells is flagged (Fig. 4b). At pixel level, the grey patch was 93.3 % snow (as a share of pixels clear on both dates) on 5 October and 0 % on 13 October: all its snow was lost, against a change of 7.0 % of pixels in the fake pair. Face A was 33.9 % snow on 5 October and 38.9 % on 13 October; 6.7 % of its pixels lost snow and 11.7 % gained it, against 15.2 % lost in the fake pair. Face A is unchanged, although only 38 % of it was clear on both dates. Face B went from 47.7 % snow to 0 %, but this shaded, steep face also changed by 29.2 % of pixels in the fake pair, so its own pixel result is weak.

An upper track above face B. A second cluster of 15 cells (0.10 km²) runs up the slope from face B to 6,350–6,600 m (centre 28.5377° N, 84.9320° E; "C2" in Figs. 3 and 4). It lies on and beside the hanging glacier above face B. I tested whether this place changes in ordinary weather. In five Sentinel-2 pairs taken before the event in which all 15 cells were clear (6 → 11, 11 → 21 and 6 → 21 October 2025; 12 → 24 August 2026; 1 → 3 October 2026), the median snow loss in C2 was 0.00 and no C2 cell was flagged (Fig. 4c). In the Sentinel-2 pair 3 → 11 October 2026, C2 had already partly lost its snow by 10:42 on 11 October (median 0.32; 3 of 13 valid cells flagged). By 13 October, Landsat 9 shows a median loss of 1.00. Part of the difference between 0.32 and 1.00 may come from the change of sensor, and part may be further change after 11 October; these cannot be separated. Clusters of this size do appear by chance elsewhere at this height: one did in 1 of 10 pre-event pairs, 3.7 km away. So the size of C2 alone is not evidence. Its location and timing are what support it. On 13 October, before this analysis, I had marked three possible failure points by eye on the January 2026 image in Google Earth. One of them (28.5392° N, 84.9341° E, about 6,600 m) lies inside C2. I chose it because dark spots, which I read as rock showing through the ice, lay on a steep part of the slope. Sentinel-2 images from the late seasons of 2020–2025 show persistent rock outcrops 200–300 m around this point, although the point itself was snow or ice at 10 m on every date. A second (4,808 m) lies 70 m from the point where the routes from faces A and B meet. The third lies on a slope that drains east, out of the Ungilung basin, and is ruled out.

Independent analyses agree on the place. The source area outlined in an ICIMOD analyst's public post (Bikas, 2026) covers 79 % of face B and 92 % of the small patch below it, but none of face A, by my approximate digitisation. The Flood Forecasting Division places the failure zone at 5,500–6,500 m (HWRRC, 2026). The NDRRMA report gives a snow avalanche at about 6,000 m and a landslide including glacier ice at about 5,500 m (NDRRMA, 2026b).

Table 1. Source-area tests. "Event" is the pair spanning 11 October; "fake" is a pair from before the event.

Test	Face A	Face B side	Glacier grey patch / main block	Control
S2 strict snow → rock, 1/6 → 11 Oct	0 %	19 % of clear pixels	0.21 km² patch	0.0 % (steep faces)
Top of change (S2, 1 → 11 Oct)	foot only (5,900–6,000 m)	from 6,200–6,300 m	total below 5,700 m	≤ 5 % above 5,300 m
S1 coherence, descending, event vs before	0.22 → 0.26	0.21 → 0.10 (43 px)	0.20 → 0.21 (at floor)	0.21 → 0.22
S1 coherence, ascending 3 → 15 Oct vs before	0.47, unchanged	0.36 → 0.20, within record (0.15–0.81)	0.44 → 0.23; difference from control lower than in only 3 of 7 earlier pairs	10.8 % of steep windows dropped as much as face B
S2 median red reflectance, 21 Oct 2025 → 21–26 Oct 2026	0.12 → 0.09–0.10	0.17 → 0.11	0.48 → 0.06	–

Test	Face A	Face B side	Glacier grey patch / main block	Control
S2 dark-area rule against 1 Oct 2026 (21–26 Oct)	0.10 km² inside (seasonal)	not reached (0.47 km away)	0.20 of 0.21 km² inside a 0.85–1.03 km² dark area	–
Landsat 9, pixels snow → not snow (% of clear pixels), event / fake	6.7 % / 15.2 %	47.7 % / 29.2 %	93.3 % / 7.0 %	7.4 % / 2.8 %
Landsat 9 grid, median event / fake	no cluster	C2 1.00 / not testable	1.00 / 0.00	2.5 % flagged by design
C2, S2 pairs before the event	–	0.00 in 5 of 5	–	–

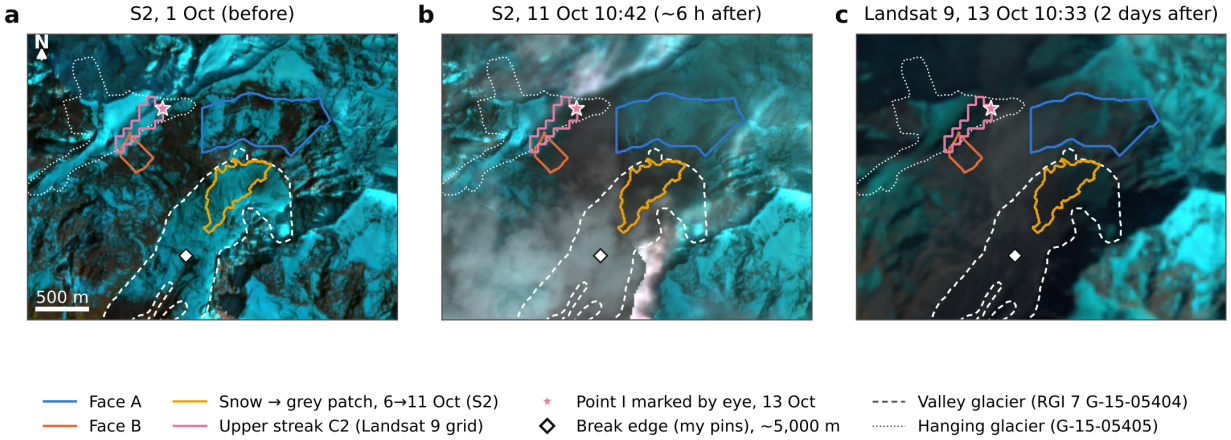


Figure 3. False-colour composites of the source area (SWIR1, NIR, green; snow and ice appear cyan, rock and debris brown or grey). (a) Sentinel-2, 1 October. (b) Sentinel-2, 11 October 10:42, partly cloudy. (c) Landsat 9, 13 October (bands 6, 5, 3). Outlines: face A (blue), face B (orange), Sentinel-2 snow → grey patch of 6 → 11 October (yellow), upper track C2 from the Landsat 9 grid test (pink), valley glacier and hanging glacier from RGI 7 (white dashed and dotted). Star: the possible failure point I marked by eye on 13 October that falls inside C2. Diamond: the break edge I marked on Google Earth images from 2006 to 2026.

The release came from the face B side. It most likely started on the hanging glacier and wall above face B at 6,100–6,600 m, and it fits NDRRMA's snow avalanche from about 6,000 m. Below this, the snow cover of the valley glacier was removed or buried over 0.31 km² at 5,020–5,470 m, which fits NDRRMA's landslide including glacier ice at about 5,500 m. Straight downhill routes from face B pass through the small patch, not the main block. The main block lies below face A, whose wall did not change. Two explanations fit. The mass from face B may have spread east across the glacier, as fast avalanches and their dust clouds do; the ICIMOD analyst reported dust over the glacier outside his source outline (Bikas, 2026). Or part of the snow, ice and debris on the upper glacier may have failed together with the mass from face B. With images at 10–30 m and no post-event DEM, I cannot tell a scar from a coat on the glacier, or measure how much ice left it.

3.3 The glacier before the event

The glacier was active and flowing up to the event (Fig. 5).

ITS_LIVE image pairs. Pairs of 5–60 days give 79 and 93 m yr^{-1} at the two fast-zone points, towards 204–208° (down-glacier). The stable rock point gives 6 m yr^{-1}. The result holds for both modern optical sensors (Landsat 8/9: 75–96 m yr^{-1}; Sentinel-2: 98–102 m yr^{-1}) and broadly for each season (63–106 m yr^{-1}). Sentinel-1 pairs give lower values (19–36 m yr^{-1}), as expected for 120 m radar tracking of a small, steep glacier. It hardly depends on pair length within 5–60 days (74–96 m yr^{-1}), which is how real motion behaves; a fixed false offset would scale as one over the pair length. From year to year, speeds were 59–98 m yr^{-1} in 2013–2021, 106–114 m yr^{-1} in 2022–2023 (a rise of about 30 %) and 75–96 m yr^{-1} in 2024. The 2025 values (47–68 m yr^{-1}) rest on few pairs. The data cube ends before 2026.

Own Sentinel-2 tracking. Independently of ITS_LIVE, the fast zone moved 114–117 m yr^{-1} in June–July 2023 and 77–132 m yr^{-1} in June–August 2025 (all above the noise threshold), towards 198–220°. In June–August 2026 the measured speeds (97–122 m yr^{-1}) were at or below the noise threshold, so they only show that the glacier was not much faster than before. Monsoon cloud covers every scene after 24 August until 30 September 2026. In the last clear pair, 1 → 6 October, the fast zone moved 2.0 m against a noise threshold of 4.1 m. Its speed was therefore below about 300 m yr^{-1}, at most about three times normal.

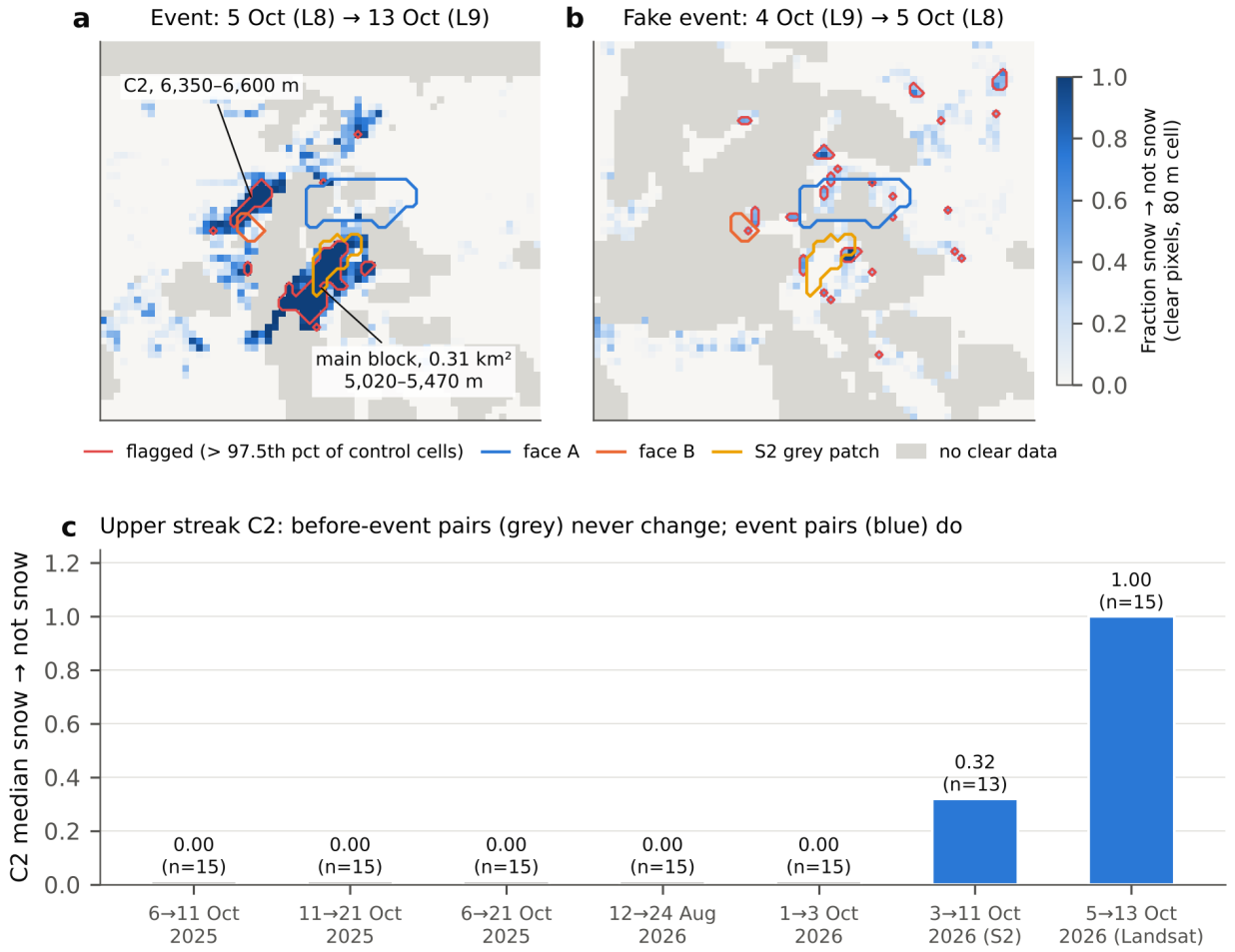


Figure 4. Grid-cell snow-loss test (80 m cells). (a) Event pair: Landsat 8, 5 October → Landsat 9, 13 October. (b) Fake pair: Landsat 9, 4 October → Landsat 8, 5 October. Red outlines: cells above the 97.5th percentile of control cells (0.98 in a, 0.35 in b). Grey: no clear data. (c) Median snow loss in the upper track C2 for five Sentinel-2 pairs taken before the event in which all 15 C2 cells were clear (grey), and for the two event pairs (blue). n is the number of valid cells.

My Google Earth pins. All five features I pinned on the glacier moved south-west between November 2016 and January 2026 (195–230°). This is the same direction as ITS_LIVE, whose layer I had hidden while placing the pins. The rock-spur control moved only 2.7 m between the 2016 and 2026 images, so the two images are well aligned. The pinned shifts (75–155 m) are much smaller than the motion expected over 9.2 years: about 730–860 m at the pair-level speeds above. A guided search, made at the positions given by the earlier (annual-composite) estimate of 470–590 m, found no trace of the 2016 features in 2026. About 500 m down-glacier the surface breaks up. I read this as the surface features being carried into the break zone, about 590 m down-glacier, and destroyed within a few years. My closer matches were look-alikes that form in the same places because the bed shapes them. So the pins confirm the direction of flow but cannot measure its speed.

A fixed break in slope. I marked the upper edge of the break-up zone on the 2006, 2008, 2016 and 2026 images, at about 84.9368° E, 28.5257° N and about 5,000 m. Between dates it moved by 9–24 m, within the precision of placing a pin on a diffuse edge. It has not moved up-glacier in 20 years. Along the flow line, the GLO-30 slope is about 28° above the edge and 34° below it. The steepest 50 m section (about 41–43°) starts at the edge (Fig. 5c). The edge is therefore fixed by the bed. My reading is that ice and debris arrive at it, break up and fall towards the gorge continuously, like a conveyor feeding an icefall, so that small ice falls there are routine. The 11 October event was a much larger release onto this active surface.

3.4 No detectable precursor

None of the tests I could make shows a precursor:

- **Speed.** The glacier showed no acceleration up to mid-August 2026, and in early October its speed was below about three times normal (Sect. 3.3).

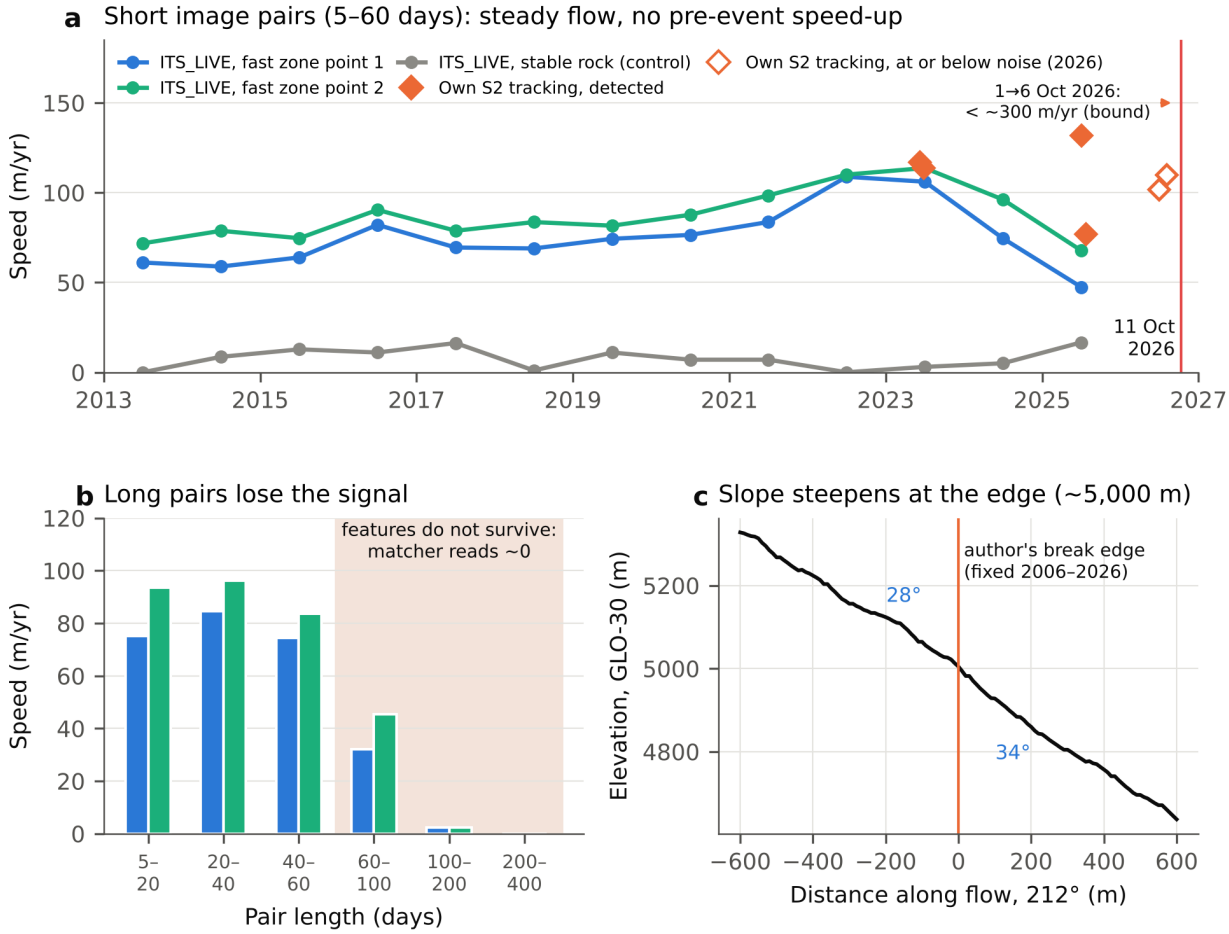


Figure 5. The glacier before the event. (a) Speed of the fast zone from ITS_LIVE image pairs of 5–60 days (vector median per year) at two points (blue, green) and at stable rock (grey), with my own Sentinel-2 feature tracking (filled: above noise; open: at or below noise). Arrow: upper bound for 1 → 6 October 2026. (b) Speed against pair length at the two points. (c) GLO-30 profile along the flow line (212°) through the break edge, with the mean slope 300 m above and below it.

- **Backscatter.** The grey patch brightened between 5 and 29 September. Other old snow and ice surfaces did the same: of 34 blocks of 500 m at 4,800–6,000 m, 19 brightened as much or more (median +2.1 dB), while bare slopes darkened. This is a region-wide change in the snow surface, such as a wet-snow phase followed by refreezing, not a change specific to the source.
- **Interferometry on face B.** In all 16 HyP3 pairs from 25 June to 11 October, the phase on face B never differed from 220–300 calibration patches by more than 2.5 robust standard deviations. The 95 % noise is 14–24 mm along the line of sight per 12 days, which is at or above the half-fringe limit of 13.9 mm. As downslope motion, the noise is about 23 mm on the ascending track and 30–51 mm on the descending track. The largest motion that can be measured without ambiguity is 18 and 30 mm. So on this small, steep face, single-pair InSAR has no detection window at all. This is the zero-width case of the "bounded at both ends" limit (Sah, 2026c, d).
- **Optical offsets on face B.** Between 24 August and 1 and 3 October, face B moved 1.0–1.5 m, at the 16th–44th percentile of 87 steep control patches. The detection floor is about 2 m per 40 days (about 18 m yr^{-1}).
- **The hanging glacier above face B.** ITS_LIVE pairs of 60–400 days give 0–2 m yr^{-1} on its Ungilung side and about 3–6 m yr^{-1} on its main body, against 0–1 m yr^{-1} on rock, up to May 2025, when the data cube ends. My own Sentinel-2 tracking between October 2025 and October 2026 found 69–89 % of glacier windows within 10 m, and the share of larger down-slope offsets (2–6 %) was the same as on rock. Same-season annual pairs can lock onto fixed shading and outcrops, so this excludes only a large acceleration, such as the rise from about 7.4 to 55 m yr^{-1} reported before the Langtang Lirung failure (Wang et al., 2026). The share of exposed rock on the hanging glacier was higher in October 2026 than in October 2025, but the new rock pixels had all been rock in earlier late seasons and lie on its western side, which drains away from the Ungilung.
- **L-band interferometry (NISAR; Fig. 6).** Coherence on the source outlines was 0.4–0.7, against about 0.2 for Sentinel-1 at the same place. On ascending track 98, face B stayed within ±1.7 cm LOS in all 11 pairs from May to September. In the last pair before the event (24 September → 7 October 05:24, four days before the collapse)

it moved +0.2 cm, less than most random patches (p ≈ 0.6–0.8). The 95 % noise level in that pair is ±1.5 cm LOS. With the estimated look geometry, this is about 3 cm of downslope motion per 12 days (about 1 m yr^{-1}). On descending track 149, the hanging glacier gave +2.1 cm (p = 0.12) in the pair that ended at 18:51 on 10 October, within its earlier range of −1.4 to +2.7 cm. Face B is mostly in shadow on this track.

- **A patch that looked like a signal.** In the 28 September → 10 October pair, a 0.8 km² patch at 5,370–6,660 m, about one-third of it on face A, gave −4.5 cm, beyond all 300 random patches in that pair. I picked this patch after looking at the map, so I tested it in every other pair. The same fixed patch reached −4.3 to +5.9 cm in the 12 earlier descending pairs (29 June → 28 September) and beat its random patches in 2 of them; in the track-48 pair that ended on 3 October it gave +2.4 cm (p = 0.23), and on the ascending track it stayed within ±0.8 cm in every pair. The evening descending passes over this steep wall are noisy, and the −4.5 cm is within this patch's normal range. It is not a precursor.

These are non-detections with stated limits. They do not show that the slope was stable.

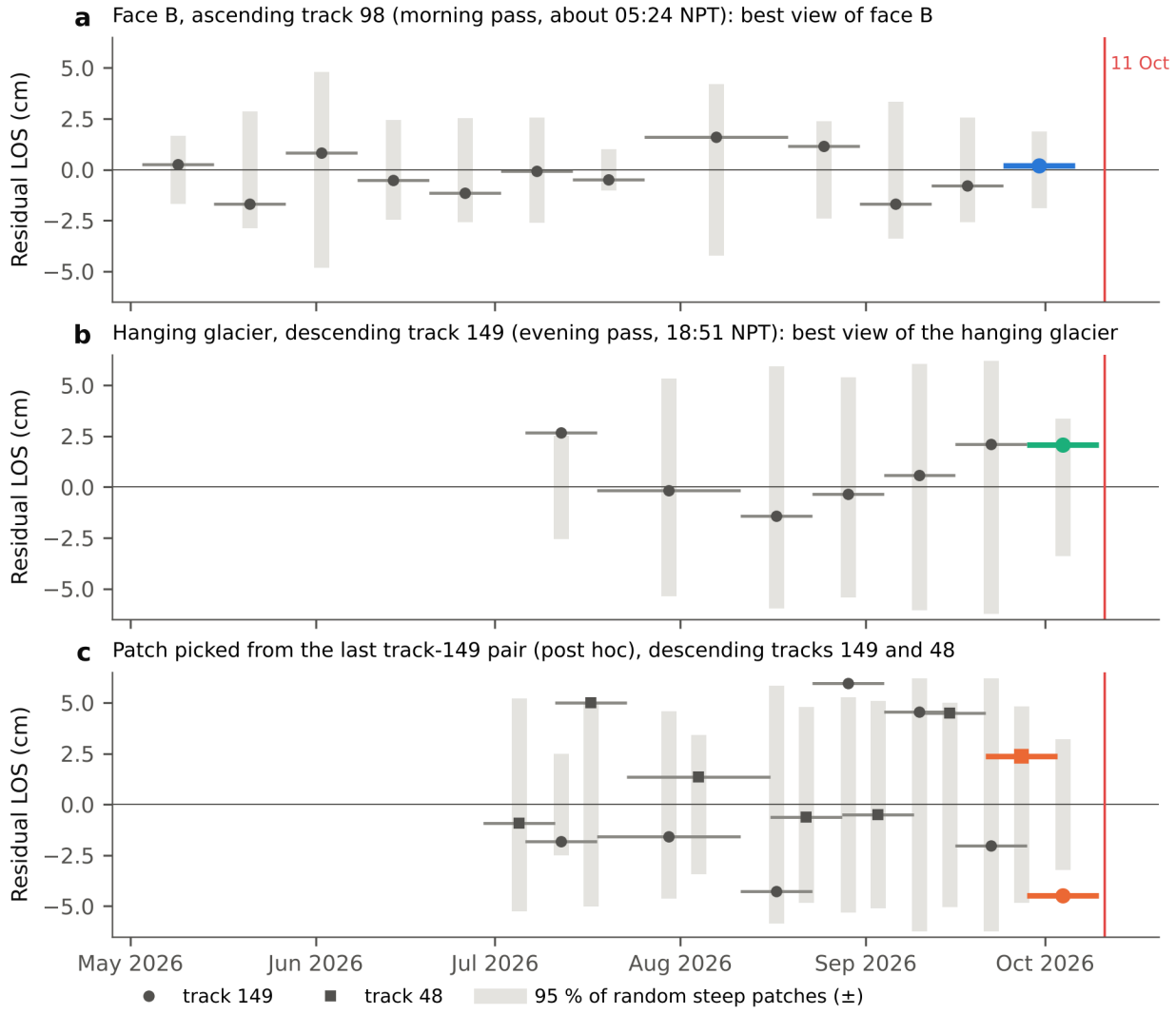


Figure 6. NISAR L-band interferograms (12-day pairs; three 24-day): residual line-of-sight displacement averaged over fixed outlines, after removing the phase that follows elevation. Horizontal bars span each pair; grey bars are the range containing 95 % of random steep patches in the same pair. Coloured: the last pair before the event on each track. (a) Face B on ascending track 98. (b) The hanging glacier on descending track 149. (c) The patch picked from the last track-149 pair, on descending tracks 149 (circles) and 48 (squares). Red line: 11 October.

3.5 Run-up on the valley walls

On 11 October, a band of vegetation loss 1–1.5 km wide followed the lower Ungilung Khola between 28.46° and 28.51° N, down to the Syar confluence (Fig. 7). In this reach it covers 4.1 km². Its height above the channel is 176 m at the median, 467 m at the 90th percentile and 657 m at the 99th percentile. Most of it lies on steep valley walls rather than the

valley floor; the grey coat mapped with the stricter deposit-type test has a median slope of 43°. The NDRRMA report states that the flow reached up to about 300 m on both banks (NDRRMA, 2026b). The report does not say whether this is a height or a distance; I compare it with heights. Helicopter video showed slopes coated by dust and a possible air blast (Petley, 2026).

From one image, I cannot separate vegetation stripped by the flow from vegetation coated by its dust cloud. The upper part of the band, more than about 300 m above the stream, is more likely dust or air-blast coating than flow. On 11 October the coated surface was dark, flat and low in SWIR, which is more like wet mud than dry dust. This agrees with the "viscous mud flow" described by NDRRMA. The clear images of 21–26 October still show the band changed (Sect. 3.8), so a dust veil that fades within days is unlikely, but at 10 m they cannot separate a lasting coat from stripped ground.

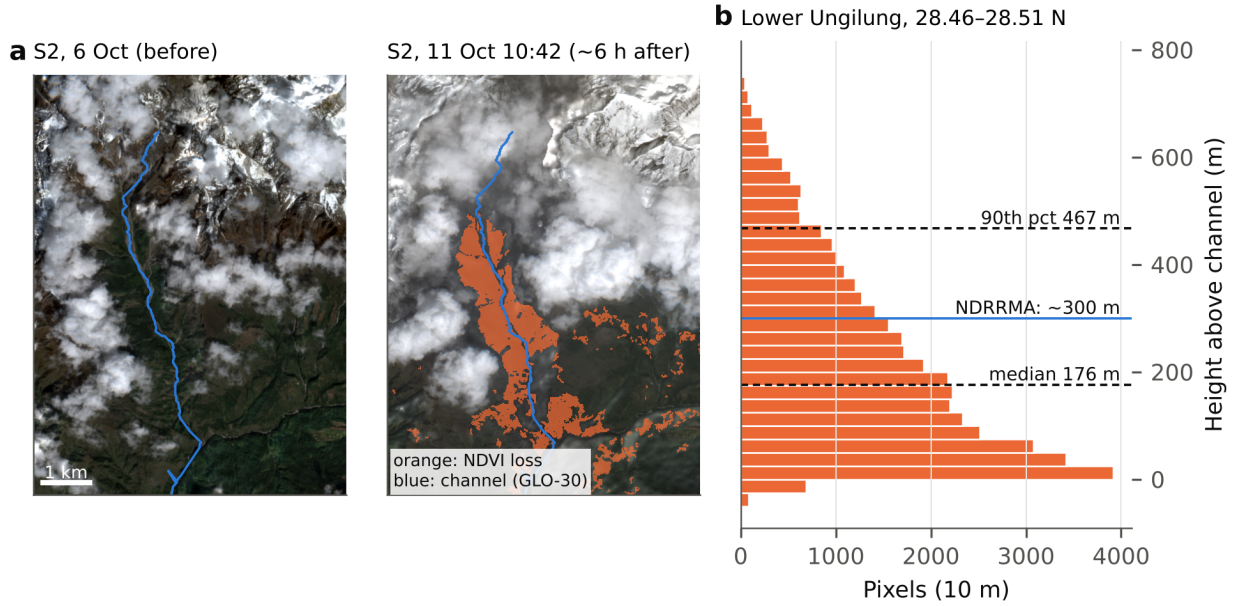


Figure 7. Vegetation loss along the lower Ungilung Khola. (a) Sentinel-2 true colour on 6 October and 11 October 10:42, with pixels that lost vegetation (orange) and the GLO-30 channel (blue). (b) Height above the channel of the vegetation-loss pixels between 28.46° and 28.51° N, with the median, the 90th percentile and the about 300 m given by NDRRMA (2026b).

3.6 The Syar Khola blockage

NDRRMA describes debris accumulating at the narrow Ungilung–Syar confluence at about 2,000 m. There, the Syar was repeatedly blocked and released. It stopped flowing about one hour before the largest flood level, and water was ponded about 1.5 km up the Syar (NDRRMA, 2026b). An eyewitness at Lokpa estimated that the Syar was blocked and released at least six times (Upreti, 2026). Situation Report 1 gives 06:15 as the time when water began flowing from the blocked section (NDRRMA, 2026a).

Three independent observations locate this blockage (Fig. 8):

- **Radar at 06:03, about 1.7 h after the collapse.** Along the Syar 0.5–0.8 km upstream of its confluence with the Ungilung, VV backscatter rose from −6.1 to −3.5 dB (+2.6 dB). At 0.9–1.5 km it rose from −6.4 to −4.6 dB (+1.8 dB). In the previous eight passes since 7 July, these reaches varied by less than ±1 dB. Further up the Syar (1.6–2.5 km), below the confluence and on the lower Ungilung, nothing changed beyond ±1 dB. The bright reach therefore ends about 1.5 km up the Syar, the distance over which NDRRMA reports ponding. It lies at 2,004–2,080 m, about 15–90 m above the confluence. Relative to the mean of the passes from 7 July to 29 September, the rises are +2.2 and +1.8 dB (Fig. 8b). A fresh, rough, wet deposit would brighten radar like this, whereas calm ponded water would darken it. So at 06:03 this reach held deposit or rough, debris-laden water, not a calm lake. This needs care, because the breach time is given as 06:15, and NDRRMA reports water ponded about 1.5 km up the Syar. The pond may have been rough or carrying debris, it may have lain where the radar cannot see into the narrow gorge, or the breach may have begun earlier: the seismic record suggests about 06:00 (Petley, 2026).
- **Sentinel-2 at 10:42.** The same reach is grey, with 82–100 % of clear pixels turned grey. In a box around the confluence the number of wet pixels rose about twelve-fold from 1 October (229 → 2,832). No open water was ponded at either confluence. On the Budhi Gandaki upstream of the Syar confluence the wet-pixel count did not change (637 → 649), so there was no backwater on the main river by 10:42.

- **The NDRRMA drone mosaic.** The mosaic of the confluence shows it filled with grey mud deposit, with ponded water at the confluence and grey deposit extending up the Syar to the east (NDRRMA, 2026b).

If the upper end of the bright reach marks the level of a temporary lake, its surface reached about 2,050–2,080 m. This would imply a blockage some tens of metres high (up to about 90 m) at the confluence. This is an inference from the position of the deposit, not a measurement. A deposit pushed up the Syar by the flow itself would look the same.

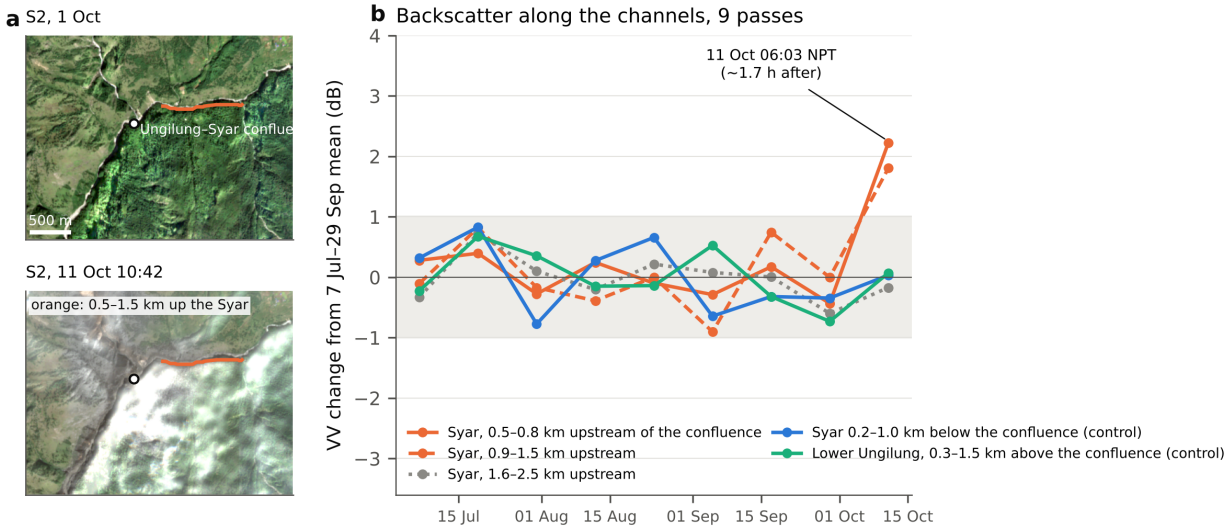


Figure 8. The Syar Khola blockage. (a) Sentinel-2 true colour on 1 October and 11 October 10:42 near the Ungilung–Syar confluence (white circle). Orange line: the Syar reach 0.5–1.5 km upstream of the confluence. (b) Sentinel-1 VV backscatter (descending track 19) along channel reaches, as the change from the mean of the passes from 7 July to 29 September. Grey band: ±1 dB.

3.7 The flood downstream

The flood reached Arughat (km 63) in at least three separate rises (Figs. 2b and 9). The NDRRMA report states that mud first reached Salleri at about 04:30 (NDRRMA, 2026b). The Flood Forecasting Division recorded a rise from 2.28 to 3.66 m at 06:30, then a slight fall. At 07:50 a second rise reached 5.01 m, above the 5.00 m danger level, and was followed by another fall. A third flood reached 6.22 m at 08:30 and 8.43 m at 08:40. The station and the bridge it was mounted on were then swept away (HWRRC, 2026). At Salleri (km 22.6), the largest level of about 20–25 m arrived at about 06:30 and swept away the hydropower camp. Smaller levels followed (NDRRMA, 2026b).

From these times and the route distances, I estimate the average speeds below. Each is an average over a long reach and depends on the precision of the times:

- **Front.** The Salleri gauge stopped at about 04:30–04:40, 24–25 km from the source, and NDRRMA gives about 04:30 for the first mud at Salleri. From a start at 04:20–04:22, a front arriving by 04:40 travelled at about 20 m s^{-1} or more, and one arriving at 04:30 at about 40 m s^{-1}. This speed is possible for a rock–ice avalanche and debris-flow front in a steep gorge, but it depends on the gauge clock and logging interval.
- **First rise at Arughat.** This rise was already under way at 06:30, about 65 km from the source. The average speed was therefore at least about 8 m s^{-1}.
- **Later waves: two alternatives.** (a) The 06:15 breach in the blockage zone (km 8–15), travelling at 8.4–9.6 m s^{-1}, would pass Salleri at about 06:30–06:40 and reach Arughat at about 07:50. In this case the breach wave is both the largest Salleri level (06:30) and the second Arughat rise, and the third, largest Arughat rise came from a later release. (b) The largest Salleri level at 06:30 is the third, largest Arughat rise (after 08:40). That wave then travelled at about 5 m s^{-1} or less, as a slower, debris-laden surge. The sparse gauge times cannot decide between (a) and (b).

The FFD estimates that the flood carried about 5.29 million m³ of extra water past Kali Khola and 4.97 million m³ past Devghat. These are estimates from rating curves, not direct measurements (HWRRC, 2026). The NDRRMA report judged that the large volume of debris from the Ungilung played a larger role in the flood level than the water ponded by the Syar blockage (NDRRMA, 2026b). My data do not test this.

3.8 The first clear images (21–26 October)

The first Sentinel-2 image with the source free of cloud was acquired on 21 October, ten days after the event. Two more followed on 23 and 26 October (Fig. 10). In a 1.5 × 1.5 km box around the main block, cloud and shadow covered 0 %

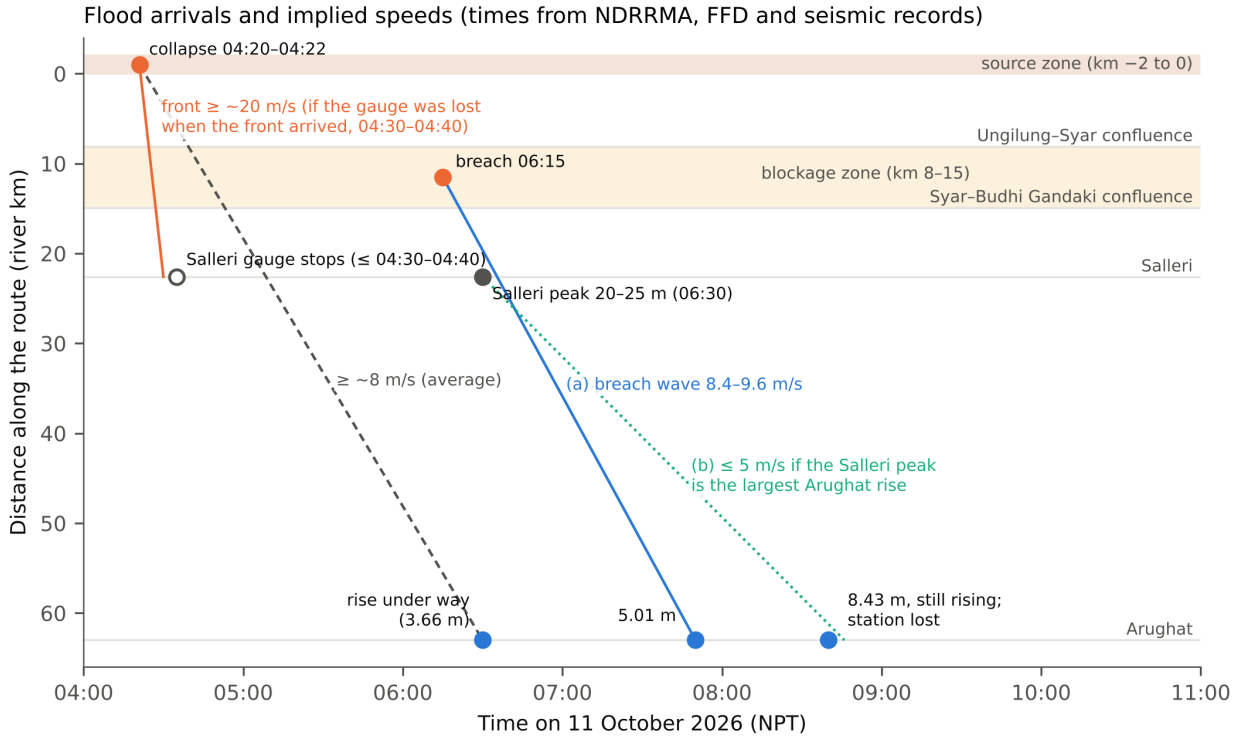


Figure 9. Distance–time diagram of the flood. River kilometres are measured from the point at 4,800 m where the routes from faces A and B meet; the source faces lie about 1.5–2 km upslope. Points are the times in Fig. 2. Lines are average speeds between them: the front to Salleri (orange) and the average to the first Arughat rise (grey). Blue and green are the two alternatives of Sect. 3.7: (a) the 06:15 breach wave reaching Arughat at 07:50; (b) the largest Salleri level reaching Arughat as the third rise.

on all three dates, and snow 14 %, 15 % and 8 %.

A dark area at the head. On the main block (the 0.21 km² snow → grey patch of Sect. 3.2), the surface was bright on 21 October 2025, the same calendar day with the same sun (median red, blue and SWIR1 reflectance 0.48, 0.45 and 0.02), and on 1 October 2026 (0.56, 0.53 and 0.02). On 21, 23 and 26 October 2026 it was dark (red 0.060–0.064, blue 0.045–0.053, SWIR1 0.035–0.046), with red above blue and more SWIR1 than before. This is not terrain shadow: the sun position on 21 October 2026 was the same as on 21 October 2025, when the surface was bright, and the local illumination modelled from the DEM (without cast shadows) shows it facing the sun. It is not shadowed snow, which is bluish, while here red exceeds blue. It is not cloud, which is bright in SWIR1, while here SWIR1 stayed low (0.04–0.05); it rose from its snow value (0.02), as a thin cover of dark debris or dust on snow and ice would make it do. With the dark-area rule (Sect. 2.3.1), the dark area around the main block covers 1.03 km² on 21 October and 1.03 km² on 23 October (the two outlines overlap with an intersection-over-union of 0.87), against the 1 October image. On 26 October the same rule gives 0.85 km² (overlap 0.61 with 21 October). I cannot tell whether this is a real change or the fixed thresholds responding to the slightly lower sun (47.0° against 48.6° on 21 October), so I give the area as 0.85–1.03 km². Against 21 October 2025 instead of 1 October 2026, the rule gives 0.55 km², because 1 October 2026 had fresh snow and part of the change against it is seasonal. The outline stayed in the same place from 21 to 26 October. Within 600 m of the main block, red reflectance changed by more than 0.08 on 8 % of pixels between 21 and 23 October and on 14 % between 21 and 26 October; I have not separated new change from differences in snow and shadow there.

The dark area covers 0.20 km² of the 0.21 km² main block and extends down the glacier and onto the slopes around it; it spans about 4,600–6,650 m (median 5,200 m). It does not reach face B (0.47 km to the west) or the small patch below it (0.17 km). It overlaps 0.10 km² (17 %) of face A, but there the change is seasonal: face A was brighter on 1 October 2026, after fresh snow, than on 21 October 2025, and after the event (red 0.09–0.10) it was close to its October 2025 value (0.12). Face B, a steep face that was partly rock in October 2025 (red 0.17), was 0.11 after the event, a small darkening that this test cannot separate from differences in snow; the small patch below it was 0.12 in October 2025 and 0.09–0.11 after. So the clear images confirm the change on the main block and the glacier below it, and confirm that face A is as it was a year earlier, but they add little about face B.

This dark area is a surface change, not the outline of the release. It is consistent with debris or dust cover, or scour, over the upper glacier. It fits both explanations of Sect. 3.2: mass from face B spreading east across the glacier, or the snow, ice and debris of the upper glacier failing with it; the optical images cannot tell them apart. That it was still there on 26 October, 15 days after the event, shows that it is not a short-lived veil, but at 10 m I still cannot tell a thin coat from a

thick deposit or from ground stripped of snow.

Changed ground down the whole path. Between 1 and 21 October 2026, the path-change rule marks 20.0 km² of changed ground in a 7.3 × 9.8 km box from the head down to the Syar confluence (Fig. 11). Most of it (15.5 km²) is vegetation lost or turned grey on the valley walls and floor. In the same weeks of 2025 the same rule gives 8.4 km², of which 5.6 km² lies at 4,500–7,000 m, and only 2.5 km² is vegetation loss; the 2025 pair had more cloud (16 % of the box against 0.6 % in 2026), so its total is a lower bound. The contrast is largest at 2,500–3,500 m, with 4.21 km² changed in 2026 against 0.04 km² in 2025. In all, 16.2 km² changed in 2026 but not in 2025. Changed patches reach the southern edge of the box (28.46° N), below the Ungilung–Syar confluence, and about 0.8 km² changed within 500 m of the confluence. In a 1 × 1 km square around the coordinate given for Chumchet by Petley (2026), which is the village on its terrace and not the source, only 0.035 km² changed. Viewing the images of 12 August, 6, 11 and 21 October in the Copernicus Browser, I saw the ground from the lower Ungilung up to the head as muddy, dark and deformed. In my lower box, drawn by hand on that view (georeferenced from a screenshot to about ±300 m), 61 % of the area changed in 2026 against 4 % in the 2025 control; in my upper box over the head the simple rule cannot separate the event from the large seasonal snow changes (17 % against 19 %), and the dark area above is the evidence there.

The Budhi Gandaki at the Yaru Khola mouth. About 4–5 km below Salleri (about river km 27), where the Yaru Khola hydropower project's Bailey bridge was reported damaged (SANDRP, 2026), the valley floor changed between 1 and 26 October. Upstream of the mouth the wide river bar turned from light beige to darker grey, and at and below the mouth the bright area along the banks widened: 31 % of pixels within 300 m of the mouth brightened by more than 0.05 in red, against 6 % of the 3 × 3 km view. This fits fresh sediment and widened channel margins. Single boulders and the bridge are below the 10 m pixel size.

3.9 NISAR coherence across the event

The three post-event NISAR pairs give a cloud-free view of the same path (Fig. 12). Below 4,000 m, on the lower Ungilung valley and its walls, coherence fell in the event pair on 12.7 % (track 48), 16.5 % (track 98) and 18.3 % (track 149) of pixels in the Sentinel-2 path-change zone. In the pre-event pairs of the same tracks, the share was at most 5.8 %, 8.7 % and 10.4 %, and at the same heights more than 1.5 km outside the path the event pairs lost only 1.5 %, 1.2 % and 2.5 %. Snow is unlikely to cover this ground in mid-October, and the control shows no scene-wide loss. Between 4,000 and 5,000 m and above 5,000 m, the event pairs did not stand out from the pre-event pairs on any track.

At the head, the dark area of Sect. 3.8 lost coherence on 10.5 %, 9 % and 4.6 % of pixels on tracks 48, 98 and 149, within the 12.6 %, 24 % and 9.3 % reached by chance in pre-event pairs. Its coherence before the event was moderate (median 0.41–0.46) and varied from pair to pair, and every event pair includes some fresh snow at this height (at least that of 12 October in ERA5; Sect. 4.1). So L-band coherence maps the lower path through cloud, but it does not outline the changes at the head; the optical images do. These are provisional products, and the event pairs span 12 days, so the loss includes any change up to 15, 19 or 22 October.

4 Discussion

4.1 The sequence of events

Putting the results together, I propose the following sequence, with the evidence for each step:

1. **Release on the face B side (about 6,100–6,600 m)** at about 04:20 on 11 October. Evidence: the highest change, a coherence loss on the descending track only (not repeated on the ascending track; Sect. 3.2), and the upper track C2 tested against pre-event pairs, together with the NDRRMA avalanche height and the seismic signal.
2. **Impact on the active valley glacier at 5,000–5,500 m.** Snow was removed or buried over 0.31 km², down to the fixed break in slope at about 5,000 m. NDRRMA reports glacier ice in the debris.
3. **Passage through the gorge and down the steep Ungilung (mean gradient 35 %)** as a highly mobile debris flow and mud flow. Its coating reached about 300 m or more up the walls, and the front passed Salleri within minutes.
4. **Blockage of the Syar Khola at its confluence with the Ungilung**, with deposit, and probably ponding, up to about 1.5 km up the Syar. The blockage breached at about 06:00–06:15, and witnesses report repeated releases.
5. **At least three rises at Arughat**, the largest last, with an excess water volume of about 5 million m³ (FFD estimate). NDRRMA judged the stage to be driven mainly by debris.

The weather gives context but no trigger. In ERA5 at the grid point nearest the source, September 2026 had 443 mm of precipitation, the wettest September in 2014–2026 (2014–2025 median 278 mm; previous maximum 404 mm in 2016). It was followed by a cold 1–9 October (mean −6.8 °C, the second coldest of these years), dry until 6 October, with 21.0 mm of precipitation, mostly as about 12 cm of snow on 7–9 October, and 4.4 mm of rain. On 10 October ERA5 gives 3.8 mm, mostly as about 2 cm of snow, with a mean of −8.2 °C, and on 11 October 0.3 mm and −10.0 °C; on 12

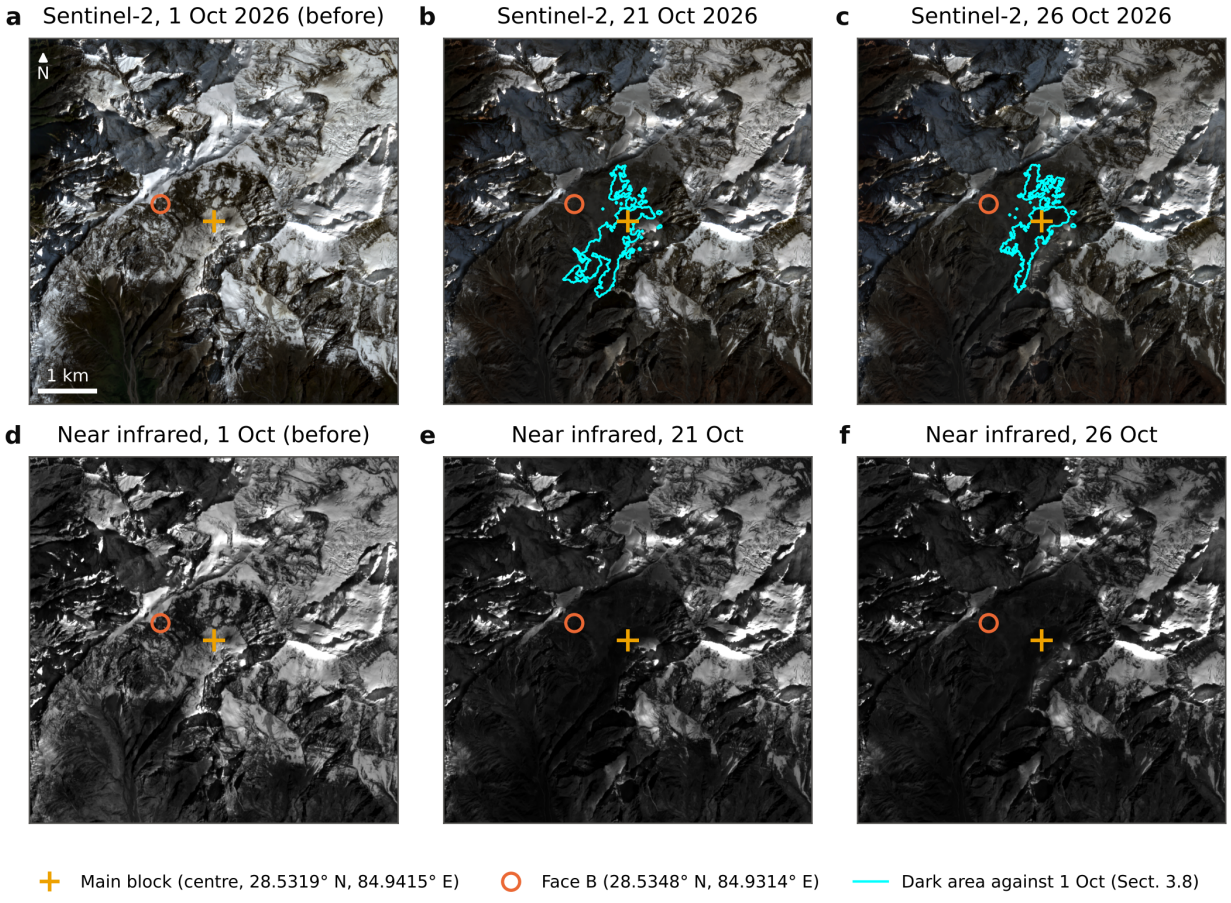


Figure 10. The head of the Ungilung Khola before and after the event (6.6 × 6.6 km, north up). **(a–c)** Sentinel-2 true colour on 1 October (before), 21 October and 26 October 2026, with the dark area against 1 October (cyan; Sect. 3.8). **(d–f)** Near infrared on the same dates. Yellow +: centre of the main block; orange circle: face B.

October, after the event, it gives about 1.6 cm of snow. The daily maximum stayed below 0 °C on every day from 4 to 12 October. So the last days before the collapse brought no more than trace rain (0.7 mm on 10 October), no warm spell and no heavy snow at this grid point. A wet September may have added water to rock joints and to the glacier bed, and snow load at high altitude, but this is a possible conditioning factor, not a measured precursor. Reanalysis precipitation over steep mountains at about 25 km resolution is uncertain, so the ranking among years means more than the amounts.

On 14 October, after the first change maps had pointed to face B, I proposed a cascade hypothesis: face B failed suddenly and blocked the narrow outlet below the glacier, a first barrier lake formed and burst, and further blockages followed at the Syar confluence and possibly at the Budhi Gandaki confluence. After the glacier was found to be active (Sect. 3.3), I extended it: the release fell onto an actively flowing, possibly saturated glacier. The source on the face B side and the active glacier were known when the hypothesis was made, so they do not test it. The later data test its other parts. At least one blockage, at the Syar confluence, is confirmed, and the floods arrived in several rises. Other parts remain untested or unsupported:

- **Lakes before 11 October.** A lake held for days before the collapse is not supported. The Salleri gauge shows no pulse, and on 6 October there was no ponded water at the 4,100 m gorge or at the confluence. On 1, 3 and 6 October, the Ungilung and Syar channels showed the same water signal as in October 2025, with no dry reach or pond.
- **A chain of lakes.** A chain of many lakes has not been tested. The 4,100 m gorge was under cloud on 11 October, and I have not searched the clear images of 21–26 October for lake remnants.
- **The water content of the glacier.** I have no measurement of whether the glacier was saturated.
- **A blockage of the Budhi Gandaki.** A barrier on the main river at the Syar confluence is possible: NDRRMA suggests it, and in alternative (a) of Sect. 3.7 the third Arughat rise needs a later release. But any such barrier had left no backwater by 10:42.

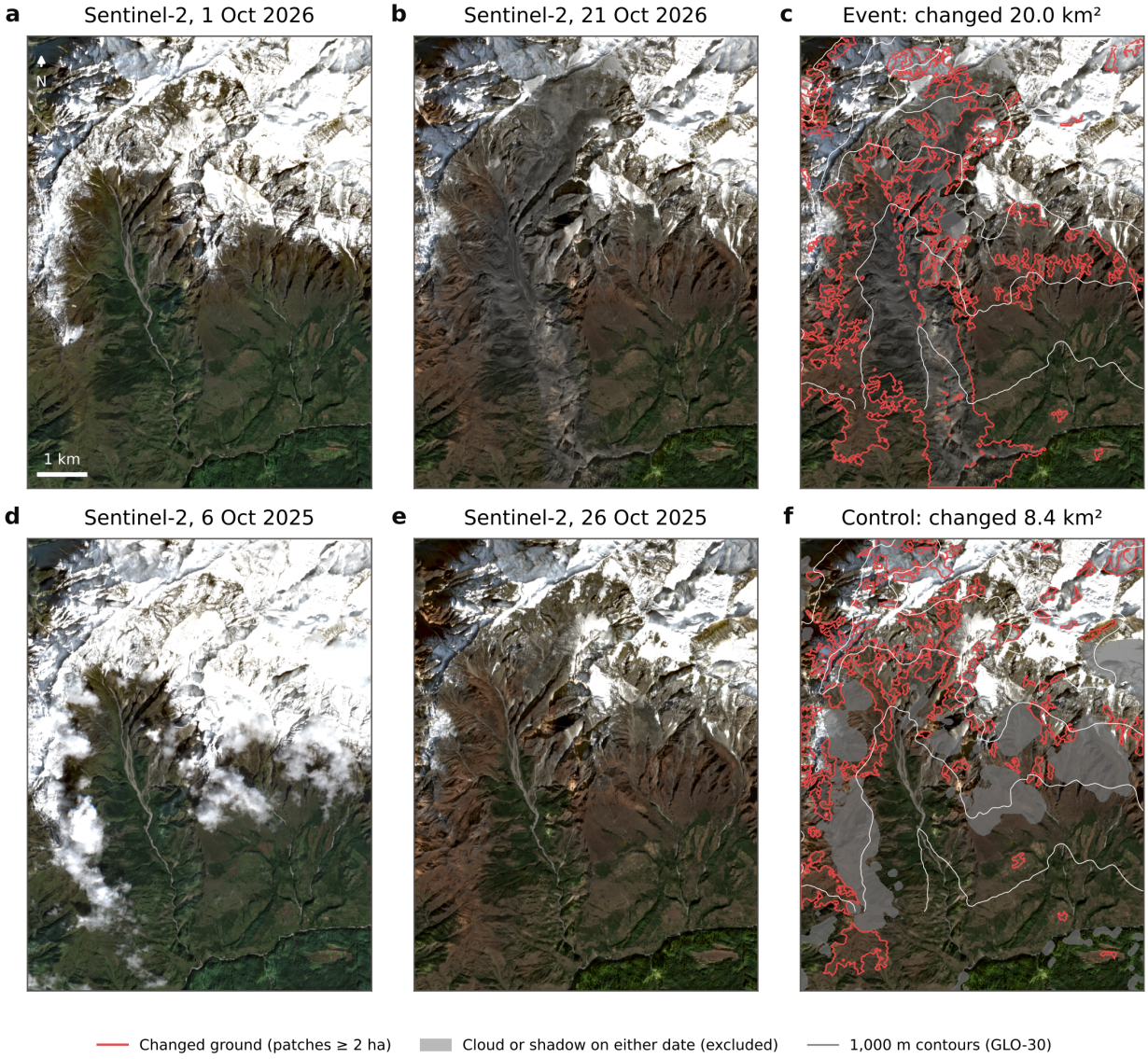


Figure 11. Changed ground along the path, from the head to below the Ungilung–Syar confluence (7.3 × 9.8 km, north up). **(a, b)** Sentinel-2 true colour on 1 and 21 October 2026; **(c)** changed ground between them (red outlines, patches ≥ 2 ha; Sect. 2.3.1). **(d–f)** The same for 6 → 26 October 2025, the same-season control. Grey: cloud or shadow on either date, excluded. White lines: 1,000 m contours (GLO-30).

4.2 Comparison with other analyses

The NDRRMA and FFD reports and the ICIMOD analyst's posts were prepared independently of this study. They agree on the place: the head of the Ungilung, between Chamar and Syerangi Himal, at 5,500–6,500 m, with face B and its gully outlined by the ICIMOD analyst. On timing, the analyst's first post proposed 5 October. In a second post the next day, the same analyst reported that imagery of 12 October showed clear evidence of a rock avalanche and glacier collapse (Bikas, 2026; SANDRP, 2026). The FFD report describes extensive new snow on the high ground in the 11 October Sentinel-2 image (HWRRC, 2026), which agrees with the fresh-snow signal that limited the radar tests (Sect. 4.3). The free 10 m data, the seismic record and the Salleri gauge all point to the early morning of 11 October.

Name usage also differs between sources: "Shringi Himal", "Siringe Himal", "Serang Himal" and "Syerangi Himal" all appear. NDRRMA places the source between Chamar Himal and Syerangi Himal, while the ICIMOD analyst and NDRRMA Situation Report 1 name the source peak Shringi or Siringe Himal. All point to the same headwall. The stream is spelled Ungilung, Ungdilung or Uingulung. I use Ungilung, following most English-language reports. The Syar Khola is also written Shyar Khola; I use Syar.

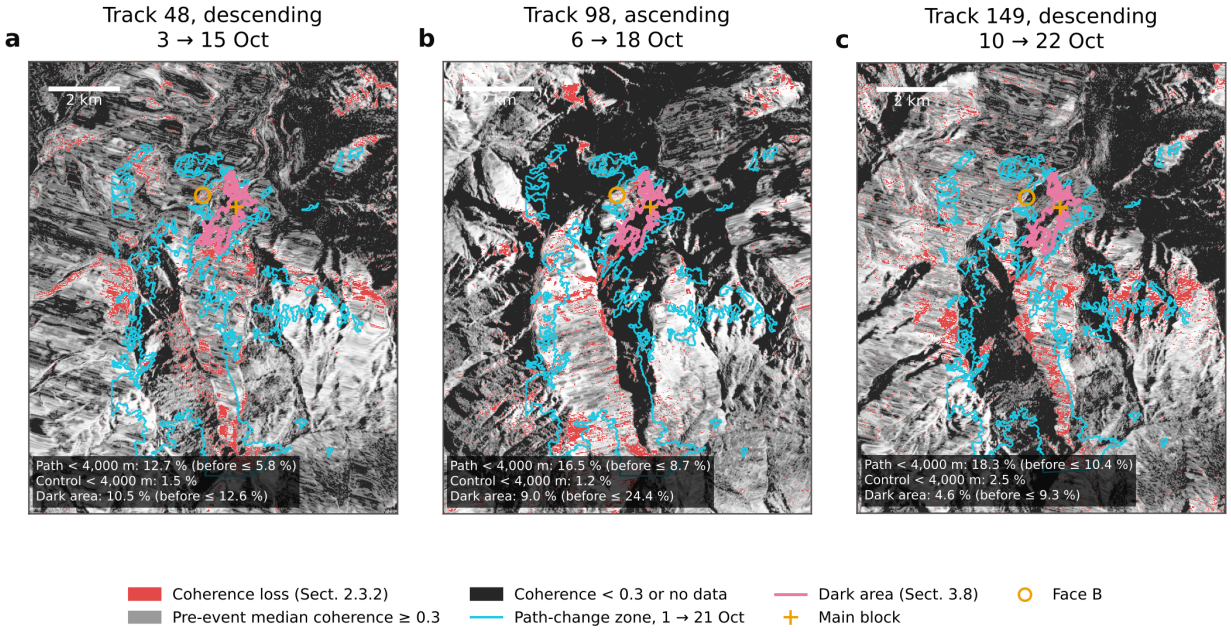


Figure 12. NISAR L-band coherence loss across the event on **(a)** track 48 (descending, 3 → 15 October), **(b)** track 98 (ascending, 6 → 18 October UTC) and **(c)** track 149 (descending, 10 → 22 October). Red: loss pixels (Sect. 2.3.2); grey: pre-event median coherence ≥ 0.3; dark: lower coherence or no data; cyan: Sentinel-2 path-change zone; pink: dark area (Sect. 3.8). The boxes give the shares of loss pixels below 4,000 m in the path zone and in the control zone, and in the dark area, with the largest share in the pre-event pairs ("before").

4.3 What free data could and could not see

Cloud. Cloud set the pace of the analysis. On 11 October, 84 % of the regional Sentinel-2 scene was cloudy. The zone between the glacier and the valley, at 4,200–5,550 m, was not clear on 11 October. Landsat 9 on 13 October was the first usable optical image of the head. The first Sentinel-2 image with the source clear came on 21 October, ten days after the event, and only then could the dark area on the upper glacier be mapped (Sect. 3.8).

The coherence floor. Radar coherence was at its noise floor (about 0.2) over the glacier and the valley before the event. A loss there cannot be measured. A grid search for coherence loss found nothing in either face, and the only clear coherence result (face B, descending track only) rests on 43 pixels and was not repeated on the ascending track. This is the same limit I found at Langtang Lirung (Sah, 2026b).

L-band. NISAR coherence on the same slopes after 12 days was 0.4–0.7, two to three times the Sentinel-1 floor, so L-band could measure the phase where C-band could not. Two limits remain. First, geometry: no single track sees the whole headwall, and the descending tracks see face B only at a grazing angle. Second, the atmosphere: on this wall the evening descending pairs swung by ±4–6 cm in quiet months, close to the ±6 cm limit of one wrapped cycle, while the morning ascending pairs stayed within about ±2 cm. These products are provisional, the ionospheric correction supplied with them was not applied, and the look geometry is estimated. After the event, L-band coherence picked out the lower path on all three tracks (Sect. 3.9), including the ascending one, on which C-band did not (Sect. 3.2), but it did not outline the source, where pre-event coherence was only moderate and fresh snow lay in every event pair.

Picking a target after looking. The −4.5 cm patch (Sect. 3.4) beat all 300 random patches in its own pair, and it would have looked like a precursor if tested only there. Tested against the same patch in other pairs, it was ordinary. Every target I report here was either defined before the NISAR data were read (faces A and B, the main block, the hanging glacier) or tested in every pair.

Backscatter. Backscatter at the head changed widely between 29 September and 11 October. In a grid test, 58 control cells were flagged against 6 in the fake pair, probably because of fresh or wet snow. This masked any scar signal. In the narrow Syar gorge, however, backscatter gave the clearest cloud-free evidence of the blockage.

ITS_LIVE annual composites. These gave a false 20-fold speed-up of the glacier from about 3 to about 80 m yr^{-1} after 2018. On this fast, strongly deforming icefall, pairs of 60–100 days lose part of the signal and pairs longer than 100 days read near zero (Fig. 5b). In the early years these long Landsat pairs dominate the composites, and in later years many short Sentinel-2 pairs dominate. Only the pair-level analysis shows that the flow was broadly steady. The acceleration was recorded in the working notes for this study and withdrawn after the pair-level test.

Quality masks at high altitude. A simple reflectance threshold on the Landsat cirrus band (band 9), which I first used

as a cirrus mask, flagged all high snow, although these pixels were not colder in the thermal band than clear pixels. The cirrus bit of the quality band flagged none of them. The CFMask cloud-shadow and dilated-cloud flags (Foga et al., 2017) masked the steep, shaded face B. For a source area above 5,000 m, I therefore used only the high-confidence cloud bit.

Fake-event tests. These were essential. Without them, a cluster the size of C2, a change on the shaded face B, or the backscatter change across the head would each look like evidence. The fake pairs show which changes happen in ordinary weather and which do not.

4.4 Limitations

- **Release scar.** I cannot map the release scar or measure the thickness of the failed mass. The pixels (10–30 m) are too coarse, and there is no post-event elevation model.
- **Volume.** The volume of rock, ice and debris is unknown. The 5 million m³ is excess water volume from rating curves.
- **The upper track C2** is supported by its location and timing, but it is not confirmed. High-ridge wind scour is less likely, because the same spot did not change in five clear pre-event pairs, but it is not excluded.
- **Coating or removal.** On the glacier and the valley walls I still cannot separate coating from removal. The dark area and the changed path persisted from 21 to 26 October, but 10 m images cannot measure thickness.
- **Change rules.** The dark-area and path-change rules use simple fixed thresholds. Their areas change with sun angle, satellite and the reference date (0.55 km² against 2025 and 0.85–1.03 km² against 1 October 2026 for the dark area).
- **Landsat pairs.** The Landsat event and fake pairs differ in processing level, mask and time span (Sect. 2.3.1).
- **Official and press records.** Times, levels and volumes come from these records and carry their own uncertainties. They include the gauge clocks, the half-hourly gauge readings, the “about 300 m” run-up and the press spelling of names.
- **An excluded result.** One pair in late June 2026 suggested a 13–15 m shift of face B. It failed a consistency test with overlapping pairs, so I do not use it.
- **Scope.** Version 2 adds the first clear Sentinel-2 images, the Sentinel-1 ascending pair of 3 → 15 October and the first NISAR pair across the event on each track. The NISAR coherence outlined the lower path but not the scar, which version 1 had expected it to show. Published high-resolution imagery or a post-event elevation model would be needed to map the release scar and estimate the volume.

5 Conclusions

1. The Ungilung rock–ice avalanche happened at about 04:20 on 11 October 2026. The Sentinel-2 change at the source lies between 6 October 10:41 and 11 October 10:42. A river gauge 23 km downstream shows no flood pulse in the six days before. The data do not support an earlier event on 5 October.
2. The release came from the face B side of the headwall, probably from 6,100–6,600 m. The snow cover of an active valley glacier was removed or buried over 0.31 km² at 5,020–5,470 m. Face A did not change. Fake-event tests support both the main block and an upper track that contains one of three possible failure points I had chosen by eye before the analysis. The first clear images, from 21 to 26 October, show a 0.85–1.03 km² dark area centred on the main block, where bright snow had turned to a dark surface, while face A was as in October 2025.
3. The glacier had flowed at about 60–130 m yr^{-1} for at least a decade, with a modest rise in 2022–2023, into a break in slope at about 5,000 m that has not moved since 2006. No speed-up, radar change or offset was detected before the event, within stated limits. Newly public NISAR L-band interferograms kept face B within about ±2 cm along the line of sight per 12 days up to four days before the collapse, and showed nothing unusual on the hanging glacier above it in the pair ending 9.5 hours before the collapse.
4. A fresh rough surface 0.5–1.5 km up the Syar Khola, seen by radar at 06:03 and most likely deposit or debris-laden water, locates the reported blockage at the Ungilung–Syar confluence. The flood reached Arughat in at least three rises, the largest last.
5. Changed ground covered about 20 km² from the head to the Syar confluence, against 8.4 km² in the same weeks of 2025. NISAR L-band coherence across the event marked the lower path below 4,000 m on all three tracks, but not the source.
6. Before a clear image arrives, free data can fix the timing and narrow the source to one face, if each change test is run against a fake event. Annual velocity composites and some quality masks can mislead in this terrain.

Code and data availability

The analysis scripts, figure scripts and derived data, with a script that recomputes the key reported values, are archived on Zenodo (Sah, 2026e; https://doi.org/10.5281/zenodo.23393209, all versions; version 1.1.0 adds the scripts and checks of version 2). Sentinel-1, Sentinel-2 and Landsat data are freely available from the Microsoft Planetary Computer, the Earth Search catalogue and USGS EarthExplorer, NISAR products and HyP3 processing from the Alaska Satellite Facility, ITS_LIVE data from NASA JPL, ERA5 through the Open-Meteo archive, and the Copernicus DEM from ESA.

Competing interests

The author declares that he has no competing interests.

Acknowledgements

I thank the National Disaster Risk Reduction and Management Authority and the Flood Forecasting Division of the Hydrology and Water Resources Research Centre for publishing their reports quickly. Sentinel data are from the Copernicus programme of the European Union. Landsat data are courtesy of the U.S. Geological Survey. Velocity data were generated using auto-RIFT (Gardner et al., 2018) and provided by the NASA MEaSUREs ITS_LIVE project (ITS_LIVE, 2026). The Copernicus DEM was produced using Copernicus WorldDEM-30 © DLR e.V. 2010–2014 and © Airbus Defence and Space GmbH 2014–2018, provided under COPERNICUS by the European Union and ESA; all rights reserved. Interferometric products were processed by ASF HyP3 (Hogenson et al., 2020). NISAR data are from the NASA–ISRO SAR mission, provided by NASA/JPL and distributed by the Alaska Satellite Facility. ERA5 data are from the Copernicus Climate Change Service, accessed through Open-Meteo.

Financial support

The author declares that no financial support was received for this study.

References

Bikas, S.: Posts on LinkedIn on the Budhi Gandaki event, 12 and 13 October 2026 (summarised in SANDRP, 2026), 2026.

Copernicus Data Space Ecosystem: Copernicus Browser, https://browser.dataspace.copernicus.eu (last access: 21 October 2026), 2026.

Element 84: Earth Search STAC API v1, collection sentinel-2-l2a, https://earth-search.aws.element84.com/v1 (last access: 30 October 2026), 2023.

ESA (European Space Agency): Copernicus DEM, ESA [data set], https://doi.org/10.5270/ESA-c5d3d65, 2022.

Foga, S., Scaramuzza, P. L., Guo, S., Zhu, Z., Dilley, R. D., Beckmann, T., Schmidt, G. L., Dwyer, J. L., Hughes, M. J., and Laue, B.: Cloud detection algorithm comparison and validation for operational Landsat data products, Remote Sens. Environ., 194, 379–390, https://doi.org/10.1016/j.rse.2017.03.026, 2017.

Gardner, A. S., Moholdt, G., Scambos, T., Fahnstock, M., Ligtenberg, S., van den Broeke, M., and Nilsson, J.: Increased West Antarctic and unchanged East Antarctic ice discharge over the last 7 years, The Cryosphere, 12, 521–547, https://doi.org/10.5194/tc-12-521-2018, 2018.

Guizar-Sicairos, M., Thurman, S. T., and Fienup, J. R.: Efficient subpixel image registration algorithms, Opt. Lett., 33, 156–158, https://doi.org/10.1364/OL.33.000156, 2008.

Hersbach, H., Bell, B., Berrisford, P., et al.: The ERA5 global reanalysis, Q. J. Roy. Meteor. Soc., 146, 1999–2049, https://doi.org/10.1002/qj.3803, 2020.

Hogenson, K., Kristenson, H., Kennedy, J., Johnston, A., Rine, J., Logan, T., Zhu, J., Williams, F., Herrmann, J., Smale, J., and Meyer, F.: Hybrid Pluggable Processing Pipeline (HyP3): A cloud-native infrastructure for generic processing of SAR data, Zenodo [code], https://doi.org/10.5281/zenodo.4646138, 2020.

HWRRC (Hydrology and Water Resources Research Centre, Flood Forecasting Division): Situation Report–1: Cause of the unusual flood in the Budhi Gandaki River and impacts on downstream areas (in Nepali), 2083-06-25 (11 October 2026), https://hydrology.gov.np/cm/files/Situation_Report_1_Budhi_Gandaki_Flood_11Oct%20Final_1791789244527.pdf, 2026.

ICIMOD: Second major Himalayan flood in seven weeks raises alarm over compounding mountain hazards, press release, Kathmandu, 13 October 2026, https://www.icimod.org/press-releases/second-major-himalayan-flood-in-seven-weeks-raises-new-questions-about-mountain-risk/, 2026.

ITS_LIVE: NASA MEaSUREs Inter-mission Time Series of Land Ice Velocity and Elevation, version 2 image-pair velocity data cubes [data set], https://its-live.jpl.nasa.gov, accessed 14 October 2026, 2026.

Kathmandu Post: Budhigandaki flood: What the report says about the gap between local warnings and official records, The Kathmandu Post, 12 October 2026, https://kathmandupost.com/national/2026/10/12/budhigandaki-flood-what-the-report-says-about-the-gap-between-local-warnings-and-official-records, 2026.

Maharjan, S. B., Dangol, P., Sherpa, T. C., Shrestha, A. B., Joshi, S. P., Shrestha, F., Bajracharya, B., Thapa, A., Kayastha, Rakesh, and Kayastha, Rijan: Insights behind the unexpected flooding in the Budhi Gandaki River, Gorkha, Nepal, ICIMOD, Kathmandu, https://doi.org/10.53055/ICIMOD.1084, 2024.

Microsoft Open Source, McFarland, M., Emanuele, R., Morris, D., and Augspurger, T.: microsoft/PlanetaryComputer: October 2022 (2022.10.28), Zenodo, https://doi.org/10.5281/zenodo.7261897, 2022.

NASA/JPL NISAR Project: NISAR Provisional Geocoded Unwrapped Interferogram Product (Version 1), NASA Alaska Satellite Facility DAAC [data set], https://doi.org/10.5067/NIL2GUNW-P1, accessed 15 and 29 October 2026, 2026.

NDRRMA (National Disaster Risk Reduction and Management Authority): Gorkha–Budhigandaki Flash Flood: Search, Rescue and Relief Response, Situation Report #01, 11 October 2026, https://ndrrma.gov.np/en/situation-report/461, 2026a.

NDRRMA (National Disaster Risk Reduction and Management Authority): Gorkha–Budhigandaki flood technical report (in Nepali, with figures), NDRRMA Facebook page, https://www.facebook.com/story.php?story_fbid=1419087763671867&id=100067119697398, 12–13 October 2026, 2026b.

Onlinekhabar: An avalanche and massive landslide triggered the devastating Budhi Gandaki flood, report finds, OnlineKhabar English, 13 October 2026, https://english.onlinekhabar.com/avalanche-landslide-budhi-gandaki-flood.html, 2026.

Petley, D.: The 11 October 2026 landslide and debris flow/flood on the Budhi Gandaki River in Gorkha district, Nepal, The Landslide Blog, Eos, 12 October 2026, https://eos.org/thelandslideblog/the-11-october-2026-landslide-and-debris-flow-flood-on-the-budhi-gandaki-river-in-gorkha-district-nepal, 2026.

RGI Consortium: Randolph Glacier Inventory – A Dataset of Global Glacier Outlines, Version 6, National Snow and Ice Data Center [data set], https://doi.org/10.7265/4m1f-gd79, 2017.

RGI 7.0 Consortium: Randolph Glacier Inventory – A Dataset of Global Glacier Outlines, Version 7.0, NSIDC: National Snow and Ice Data Center, Boulder, Colorado, USA [data set], https://doi.org/10.5067/f6jmovy5navz, 2023.

Sah, A. K.: No detectable precursor in Sentinel-1 backscatter before the 26 August 2026 Langtang Lirung rock–ice avalanche, Nepal, EarthArXiv [preprint], https://doi.org/10.31223/X59N5N, 2026a.

Sah, A. K.: Calibrated detection limits in routine Sentinel-1 products 50.6 hours before the Langtang Lirung rock–ice avalanche, Nepal, EarthArXiv [preprint], https://doi.org/10.31223/X5KZ3G, 2026b.

Sah, A. K.: Bounded at both ends: the detection window of routine 12-day C-band InSAR at rock–ice avalanche sources, EarthArXiv [preprint], https://doi.org/10.31223/X58J72, 2026c.

Sah, A. K.: The single-pair unwrapping ceiling is a property of the track, not of the radar, EarthArXiv [preprint], https://doi.org/10.31223/X5GZ3J, 2026d.

Sah, A. K.: Code and derived data for: A steadily flowing glacier and no detectable precursor before the 11 October 2026 Budhi Gandaki rock–ice avalanche and flood, Nepal, Zenodo [data set], version 1.1.0, https://doi.org/10.5281/zenodo.23393209, 2026e.

SANDRP: Oct. 2026: Budhi Gandaki Flashflood Affects Four Hydro Projects in Nepal, South Asia Network on Dams, Rivers and People, 13 October 2026, https://sandrp.in/2026/10/13/oct-2026-budhi-gandaki-flashflood-affects-four-hydro-projects-in-nepal/, 2026.

Shugar, D. H., Jacquemart, M., Shean, D., et al.: A massive rock and ice avalanche caused the 2021 disaster at Chamoli, Indian Himalaya, Science, 373, 300–306, https://doi.org/10.1126/science.abh4455, 2021.

Upreti, H.: Torrent of black mud and rocks engulfs settlements along Budhigandaki, The Kathmandu Post, 12 October 2026, https://kathmandupost.com/national/2026/10/12/torrent-of-black-mud-and-rocks-engulfs-settlements-along-budhigandaki, 2026.

Uprety, H., Adhikari, P., and Kaini, S.: Five things to know about the Budhi Gandaki flash flood, The Kathmandu Post, 11 October 2026, https://kathmandupost.com/gandaki-province/2026/10/11/five-things-to-know-about-the-budhi-gandaki-flash-flood, 2026.

van der Walt, S., Schönberger, J. L., Nunez-Iglesias, J., Boulogne, F., Warner, J. D., Yager, N., Gouillart, E., and Yu, T.: scikit-image: image processing in Python, PeerJ, 2, e453, https://doi.org/10.7717/peerj.453, 2014.

Wang, T., Sassa, S., Yang, W., Li, R., Xu, C., and Qi, W.: Precursor of a powerful large glacier landslide causing tsunami floods in the 26 August 2026 Nepal disaster, Landslides, 23, 3489–3495, https://doi.org/10.1007/s10346-026-02842-6, 2026.

Zippenfenig, P.: Open-Meteo.com Weather API, Zenodo [software], https://doi.org/10.5281/zenodo.7970649, 2024.